The Seismic Structure and Dynamics of the Mantle Wedge

Douglas A. Wiens,[1] James A. Conder,[1] and Ulrich H. Faul[2]

[1]Department of Earth and Planetary Sciences, Washington University, St. Louis, Missouri 63130; email: doug@wustl.edu, conder@seismo.wustl.edu

[2]Department of Geological Sciences, Boston University, Boston, Massachusetts 02215; email: ufaul@bu.edu

Annu. Rev. Earth Planet. Sci. 2008. 36:421–55

First published online as a Review in Advance on February 12, 2008

The *Annual Review of Earth and Planetary Sciences* is online at earth.annualreviews.org

This article's doi:
10.1146/annurev.earth.33.092203.122633

0084-6597/08/0530-0421$20.00

Key Words

subduction zone, island arc volcanism, backarc basin, mantle flow, seismic tomography, seismic anisotropy

Abstract

Seismic imaging provides an opportunity to constrain mantle wedge processes associated with subduction, slab dehydration, arc volcanism, and backarc spreading. The mantle wedge is characterized by a low attenuation forearc, an inclined zone of low velocity and high attenuation underlying the volcanic front, and a broad region of low velocity and high attenuation beneath the backarc spreading center when present. Seismic velocities, bathymetry, and basalt chemistry suggest mantle temperature variations of ~100°C between different backarc regions. Rock physics experiments and geodynamic modeling are essential for interpreting seismic observations. Seismic anisotropy indicates a complex pattern of mantle flow that can be modeled with along-strike flow in a low viscosity channel beneath the arc and backarc. Comparison of geodynamic models with seismic tomographic results using experimentally derived relations between velocity, attenuation, and temperature suggests the existence of small melt fractions in the mantle at depths of 30–150 km.

1. INTRODUCTION

The wedge of uppermost mantle overlying subducting slabs is the locus of many of the most significant processes controlling the geological evolution of Earth. This region, including the forearc mantle wedge, volcanic arc, and in some cases a backarc spreading center, is vital for understanding the processes that shape our planet, including arc magmatism, the hydration of the upper mantle by volatiles from the slab, and in cases of active backarc spreading, the formation of new seafloor at spreading centers.

The production of arc magmas in the mantle wedge is an important factor in the geodynamical and geochemical evolution of Earth. Although the relative role of Phanerozoic arc volcanism in continental crustal formation is still under debate (Armstrong 1991, Tatsumi 2005, Brown & Rushmer 2006), there can be no doubt that arc crust has contributed to some extent in the formation of the current continental crust. In addition, the mantle wedge is highly important because of its involvement in Earth's volatile cycle. Water is liberated from the subducting slab by pressure- and temperature-sensitive dehydration reactions and is either taken up within the crystal structure of normally anhydrous mantle minerals (Hirschmann et al. 2005) or transported upward through the wedge in the form of hydrous minerals, a free fluid, or hydrous melts (Schmidt & Poli 1998, Iwamori 1998). Other volatiles, such as carbon dioxide, may follow similar paths. Thus, understanding volatile transport through the mantle wedge is essential to working out the mantle's volatile budget (Thompson 1992).

Finally, some intraoceanic arcs are accompanied by backarc spreading centers, so that significant quantities of new oceanic crust are produced in the mantle wedge. Although backarc spreading centers have many similarities to mid-ocean ridges, they show more rapid temporal variations in spreading rate (Jurdy & Stefanick 1983) and larger, along-strike morphological and geochemical variations (Taylor & Karner 1983, Taylor & Martinez 2003). Strong variations in volatile content of the upper mantle in backarcs (Kelley et al. 2006) and the controlling influence of the subducting slab on flow in the mantle wedge (Sleep & Toksoz 1971, Ribe 1989) may cause unique characteristics in oceanic lithosphere produced above the wedge.

Many important questions remain regarding the physical processes in the mantle wedge. These include the pattern of mantle flow, the mechanism and depth extent of melt production, the mechanics and timescale of water and melt transport, and the temperature structure of the mantle wedge. For example, there is debate about the porosity of melt-forming regions in the mantle, with widely varying estimates ranging from less than 0.01% to more than 3% (Lundstrom et al. 1998, Turner et al. 2000, Faul 2001, Nakajima et al. 2005, Turner et al. 2006), and corresponding uncertainty about the rapidity of magma extraction from the mantle. Arcs with active backarc extension introduce additional questions about the dynamics of backarc spreading centers, the relationship of backarc to arc magma production, and the similarities and differences of backarc and mid-ocean ridge spreading centers.

Seismological observations, combined with rock mechanics experiments and geodynamic modeling, have the potential to provide important constraints on the dynamics of the mantle wedge and to answer the questions noted above. In this paper we present a review of recent progress toward this goal. We first describe seismological observations constraining the structure of the mantle wedge, beginning in the forearc wedge and extending beneath the arc and backarc, including observations of seismic anisotropy. Then we describe processes affecting seismic properties of rocks, including recent progress in laboratory experiments characterizing temperature dependence and melt content. We present geodynamic models for the mantle wedge that make testable predictions about the spatial distribution of temperature anomalies and melt production in the mantle wedge. Finally, we compare seismic tomographic images with these predictions using the laboratory-derived relationships between seismic parameters and material properties.

2. SEISMIC OBSERVATIONS

2.1. Structure of the Forearc Mantle

The forearc mantle extends from where the downgoing plate first contacts the overriding mantle, usually at depths of 10 to 40 km, to just seaward of the volcanic front. This region is characterized by exceptionally low seismic attenuation, with the boundary between low attenuation and high attenuation occurring just toward the forearc side of the arc volcanoes (Roth et al. 1999, Tsumura et al. 2000, Schurr et al. 2003, Stachnik et al. 2004). Heat flow observations show uniformly low values in the forearc and a sudden transition to high heat flow in the arc (Furukawa 1993). These observations suggest a forearc characterized by cold, rheologically strong mantle and a sharp transition to warmer, lower viscosity mantle near the volcanic front (Kincaid & Sacks 1997, Conder 2005).

The seismic velocity structure of the forearc mantle wedge is more uncertain. Body wave tomographic images generally show high seismic velocity in the mantle forearc (Reyners 2006, Zhao et al. 2007) (**Figure 1**), although the outermost mantle forearc in Costa Rica shows low mantle P-velocities and high V_p/V_s ratios consistent with serpentinization (DeShon & Schwartz 2004). Active source surveys have found evidence of low seismic velocity in the mantle wedge in several arcs that are widely attributed to serpentinization of mantle peridotite by fluids from the downgoing plate. In the Mariana and Izu-Bonin regions, serpentinite diapirs and seamounts are common in the forearc (Fryer et al. 1995); a seismic refraction survey over one of them shows low velocity mantle wedge consistent with serpentinization of the outermost mantle wedge (Kamimura et al. 2002). In Cascadia, receiver function images (Bostock et al. 2002), active source seismics (Brocher et al. 2003), and potential field anomalies (Blakely et al. 2005) all suggest that the seaward edge of the forearc mantle is highly serpentinized. A possible interpretation of these observations is that the forearc mantle wedge generally shows high seismic velocities and low attenuation as a result of cold temperatures, but that variable serpentinization produces locally low velocities and anomalous V_p/V_s ratios, particularly in the outer forearc.

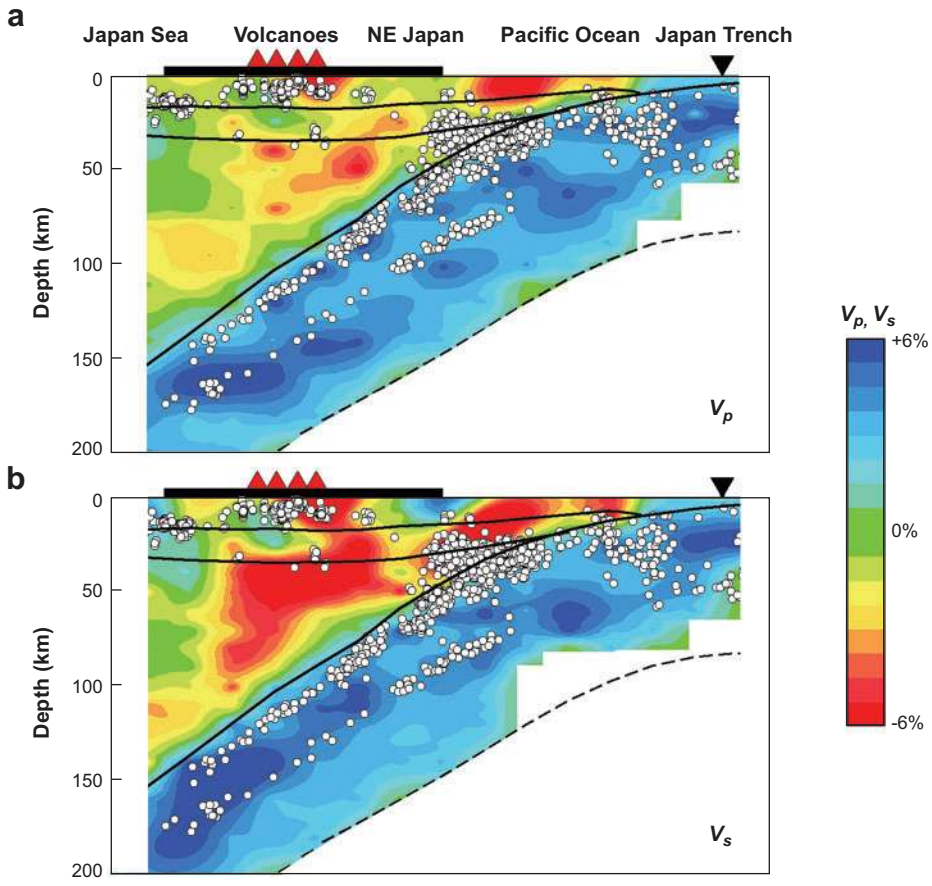

Figure 1

Vertical cross sections of P-wave (*a*) and S-wave (*b*) velocity perturbation (in percent) in northern Japan relative to an average Japan arc model (after Zhao et al. 2007). Colors denote seismic velocity anomalies, and open circles denote microearthquakes within a 15 km width along the profile. The land area and active volcanoes are shown at the top of each figure by bold horizontal lines and triangles.

2.2. Mantle Structure Beneath Volcanic Arcs

The most detailed images of seismological structure beneath volcanic arcs come from body wave tomographic images obtained by dense regional networks or temporary seismograph deployments overlying highly seismic intermediate depth slabs. Such tomographic images have now been obtained for a wide variety of mantle wedge regions with varying resolution, depending on the density of seismographs, level of seismicity, and duration of the recording. Ideally, images of P and S velocity and attenuation structure should be interpreted simultaneously because these measurements provide different types of constraints and the use of all three structures can

reduce the ambiguity in interpretation (Wiens & Smith 2003). In practice, S velocity and attenuation images are usually less detailed than P images owing to the lower number of phase arrivals in the former case and limited measurement precision in the latter.

The highest resolution images of a volcanic arc have been obtained in Japan (**Figure 1**) where there is a long history of recording with dense seismic arrays (Zhao et al. 1992, 2007; Zhao & Hasegawa 1993; Nakajima et al. 2001). Images obtained in other regions generally show similar features to the Japan images (Zhao et al. 1995, 1997; Myers et al. 1998; Graeber & Asch 1999; Gorbatov et al. 1999; Husen et al. 2003; Wagner et al. 2005; Barklage et al. 2006; Reyners 2006). Here we discuss typical features of arc tomographic images with particular reference to the well-resolved Japanese arc; prominent differences between regions are noted. Mantle wedges containing active backarc spreading centers constitute a special case and are expected to show different dynamics and structure associated with basalt production and seafloor spreading in the backarc; these are discussed in the next section.

Most well-resolved subduction systems with island arc volcanism show an inclined low-velocity, high-attenuation region above the subducting slab extending from the Moho to depths of ~150 km (**Figure 1**). The slowest velocities in this region are generally $V_p = 7.4$ km s^{-1} and $V_s = 4.0$ km s^{-1}, giving a V_p/V_s ratio of 1.85. These anomalies represent deviations of approximately –8% and –10% relative to standard global average seismic models such as IASPEI91 (Kennett & Engdahl 1991). However, they are often plotted relative to regional velocity averages, which are slower than global models, resulting in smaller percentage anomalies.

Seismic attenuation models for the mantle wedge have lower spatial resolution than velocity models but also generally show high attenuation (low Q) in the same region (Roth et al. 1999, Tsumura et al. 2000, Takanami et al. 2000, Schurr et al. 2003, Stachnik et al. 2004, Pozgay et al. 2007b). Comparisons of attenuation values between different regions and studies are complicated by various frequency bands used and different ways of treating frequency dependence (Flanagan & Wiens 1998, Stachnik et al. 2004). One approach is to normalize measurements made in narrower bands assuming a frequency-independent Q to a reference frequency of 1 Hz (Stachnik et al. 2004), using a frequency dependence exponent (α) of 0.26, consistent with both laboratory experiments and seismological measurements in the mantle wedge (Jackson et al. 2002, Flanagan & Wiens 1998, Shito et al. 2004). Using this approach, most studies suggest a minimum Q_p of approximately 100 for the upper mantle beneath an active volcanic arc.

Seismic images show higher velocities and lower attenuation in mantle wedge regions that lack an active volcanic arc, suggesting that the extremely low velocities and high attenuation found beneath volcanically active arcs are related to the process of melt production in the wedge. Amagmatic portions of the Alaska subduction zone are characterized by lower attenuation ($Q_p \sim 250$) compared with magmatically robust subduction zones elsewhere (Stachnik et al. 2004), and the V_s and V_p/V_s ratios of the Chilean subduction zone change dramatically between magmatic and amagmatic sections (Wagner et al. 2005). In northeast Japan, there is a relationship between the strongest upper mantle velocity anomalies and concentrations of

Quaternary volcanoes, suggesting that arc volcano spacing is controlled by the spacing of upper mantle melt production regions as delineated by tomography (Tamura et al. 2002).

2.3. Structure of Active Arc/Backarc Systems

Island arcs with active backarc spreading centers may be expected to show significant structural differences from volcanic arcs without active backarcs. The magma production rate needed to generate the oceanic crust at a fast-spreading backarc spreading center, such as the Lau basin (Tonga), is more than an order of magnitude greater than the magma production rate of a typical island arc, so the magmatic system for backarc spreading must be much more vigorous. In addition, backarc spreading must be part of a mantle flow pattern that has significant differences from that of a mantle wedge without an active backarc (Ribe 1989, Conder et al. 2002).

Seismic imaging of backarc systems is problematic because they are largely covered with water and thus do not have good distributions of permanent seismic stations. The Lau backarc basin behind the Tonga trench is probably the best imaged arc-backarc system owing to a large deployment of ocean-bottom seismographs (OBS) in 1994. Tomographic images show a large, low-velocity region extending from the volcanic arc to several hundred kilometers beyond the active Lau spreading center, suggesting a broad zone of high temperatures in the upper mantle (**Figure 2**) (Conder & Wiens 2006, Zhao et al. 1997). Attenuation results, inverted in this paper from the Roth et al. (1999) dataset, also show a broad region of extremely high attenuation in the upper mantle (**Figure 2**). Comparison of different tomographic results suggests that the seismic velocity and attenuation anomalies associated with backarc spreading are larger in magnitude than those associated with arc volcanism. We might speculatively attribute this to the larger melt production of backarc spreading systems.

Waveform inversion results, which provide more resolution on the depth dependence of seismic velocity at the cost of lateral resolution, show that the minimum velocity occurs at 70 km depth, consistent with the expected onset depth of primary mid-ocean ridge basalt magma production (Shen & Forsyth 1995). Assuming that the low-velocity and high-attenuation area denotes the magma production region, the Lau tomography results suggest that melt production occurs over a wide geographical region within the upper 100 km of the mantle, consistent with results from a large OBS experiment on the East Pacific Rise (Conder et al. 2002b, Hammond

Figure 2

P-wave (*a*), S-wave (*b*), and Q_p (*c*) tomographic models for the Tonga-Lau subduction zone and backarc basin from an ocean-bottom seismograph deployment. The P-wave and S-wave models are from Conder & Wiens (2006) and are given as velocity anomalies relative to the IASPEI91 velocity model (Kennett & Engdahl 1991). The Q_p structure was determined by reinverting the attenuation measurements of Roth et al. (1999) using ray paths calculated for the above velocity model. The solutions are masked where the structures cannot be adequately resolved. Circles denote earthquake hypocenter locations. CLSC denotes the position of the Central Lau Spreading Center.

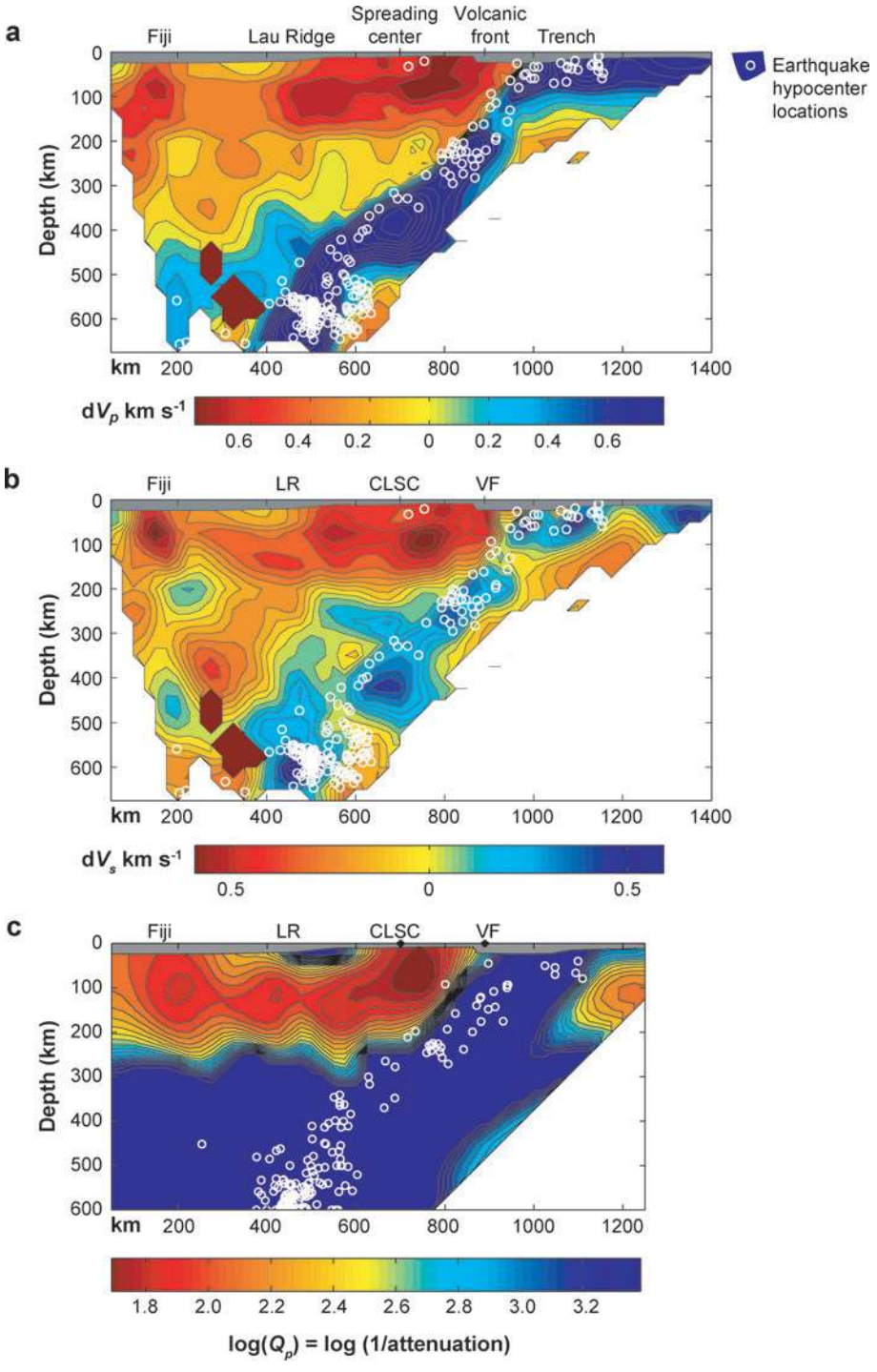

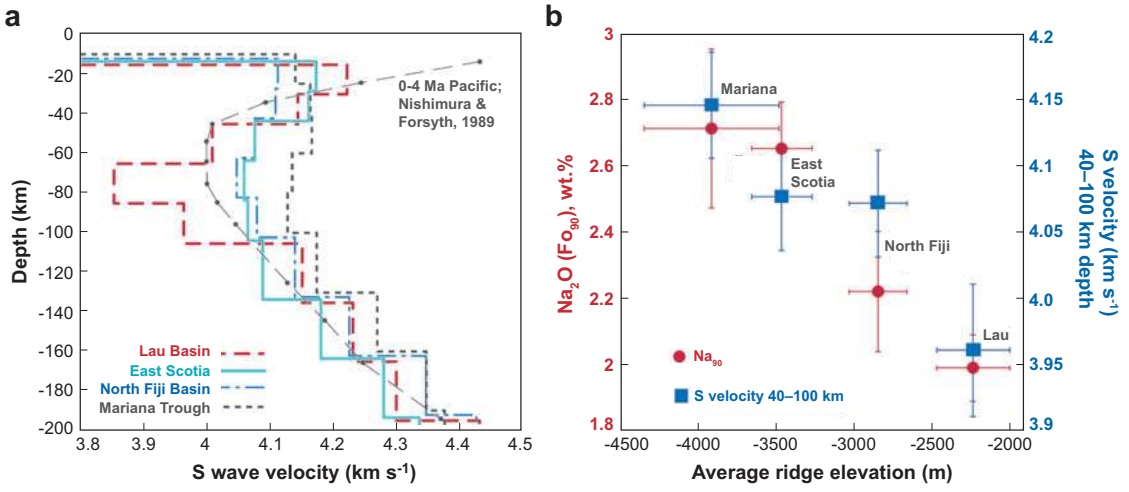

Figure 3

(*a*) Isotropic shear wave velocity structure as a function of depth determined from regional waveform inversion for each of the backarc regions (Wiens et al. 2006a). The isotropic structure of 0–4 Ma Pacific ocean lithosphere from Nishimura & Forsyth (1989) is shown, illustrating that the average mantle structure of backarc basins is similar to mid-ocean ridges. (*b*) The average S velocity between 40–100 km depth and Na_2O concentration in equilibrium with Fo_{90} are plotted as a function of average ridge depth for active backarc basins (Wiens et al. 2006a). Petrologic melting models suggest that $Na_{(Fo90)}$ concentrations are inversely correlated with temperature. The Lau Basin shows low seismic velocities, high ridge elevations, and low Na concentrations, which are all indicative of high upper mantle temperatures. Conversely, the Mariana Trough shows higher seismic velocities, low ridge elevations, and high Na concentrations, indicating cold upper mantle temperatures.

& Toomey 2003, Hung et al. 2000). This finding indicates that melt production at fast-spreading ridges occurs within a mantle flow pattern dominated by passive upwelling in response to plate motions (Scott & Stevenson 1989, Turcotte & Morgan 1993) rather than narrow buoyancy-driven upwelling, whether at mid-ocean or backarc locations.

Seismic and petrological evidence indicates mantle temperature variations on the order of 100°C between different mantle wedge regions (Wiens et al. 2006a). Seismic waveform inversion results show large variations in seismic velocity between backarcs, particularly at depths of 60–85 km (**Figure 3*a***). At this depth, the Lau backarc shows velocities approximately 7.5% lower than the Mariana backarc, with the North Fiji and East Scotia backarcs being intermediate between these extremes. The upper mantle seismic variations are correlated with spreading center elevation and basalt major element systematics (**Figure 3*b***). The Lau Basin shows unusually shallow axial depths of approximately 2200 m, whereas the Mariana backarc shows anomalously deep ridge axis depths of 3900 m and the North Fiji Basin and East Scotia backarcs show intermediate depths. The major element systematics of backarc basin basalts,

particularly their Na and Fe trends reflecting extent of melting, suggest that upper mantle temperatures are consistently warmer in the Lau Basin than in the Mariana Basin (Taylor & Martinez 2003). Wiens et al. (2006a) and Kelley et al. (2006) calculate upper mantle potential temperatures for the Lau Basin that are ∼100°C warmer than the Mariana Basin, based on major element systematics corrected for water content. To produce the large observed variation in ridge elevation, these temperature differences must extend through approximately the upper 200 km of the mantle wedge (Wiens et al. 2006a). These differences may reflect variations in the rate of backarc spreading, slab rollback, and the vigor of mantle flow, as mantle flow models suggest these factors may influence the temperature in the mantle wedge (Kincaid & Griffiths 2003).

2.4. Seismic Anisotropy and Constraints on Mantle Flow

Seismic anisotropy provides a possible constraint on the mantle flow pattern, as both upper mantle xenolith observations (Christensen 1984, Mainprice & Silver 1993) and laboratory experiments (Zhang & Karato 1995) show that shear strain associated with flow preferentially aligns olivine and pyroxene crystals in mantle peridotite. Most studies suggest that the fast direction will be aligned with the mantle flow direction (Mainprice & Silver 1993), although other interpretations are possible (see Section 3.2.2).

Seismological studies are generally not able to completely characterize upper mantle anisotropy. However, shear wave splitting observations of nearly vertically traveling shear waves offers a convenient method of studying the azimuthal orientation of subhorizontal fast and slow anisotropic axes in the upper mantle. Teleseismic SKS splitting studies often yield results that are unable to localize the anisotropy to the mantle wedge owing to the possibility of anisotropy below the slab, whereas local S splitting studies from sources near the top of the slab alleviate this ambiguity. Small magnitude splitting measurements may result from anisotropy in the crust, but many arc and backarc regions show large splitting times (0.5–2 s) that are incompatible with an origin in the relatively thin crust.

Shear wave splitting studies have now been carried out for most subduction zones and some generalizations are possible. Most volcanic arcs are characterized by along-strike fast shear wave splitting directions (Wiens & Smith 2003). **Table 1** shows the average fast axis orientation relative to subduction zone strike and the apparent motion of the subducting plate for various arcs.

Several mantle wedge regions are characterized by a prominent rotation of the fast direction of anisotropy from along-strike in the forearc or arc to arc-perpendicular in the backarc (**Figure 4**). The Tonga-Fiji region shows along-strike fast directions near the volcanic arc, which rotate to a north-south direction near the Lau backarc spreading center and to convergence-parallel (approximately arc-perpendicular) in the far backarc (Smith et al. 2001). These fast axis orientations, if interpreted as indicating the direction of mantle flow, are consistent with geochemical inferences of southward flow of Pacific mantle induced by slab rollback (Turner & Hawkesworth 1998, Pearce & Stern 2006). The Mariana arc shows along-strike fast directions in

Table 1 Fast direction and approximate magnitude of shear wave splitting in the mantle wedge

Subduction zone	Forearc	Arc	Backarc	References*
Aleutians	Arc parallel, 0.1 s	Arc parallel, 0.25 s		(Yang et al. 1995)
Alaska	APM parallel, 0.5 s	Arc parallel, 0.75 s	Arc parallel, 0.75 s	D. Christensen, personal communication, 2007
Kamchatka	APM parallel/Arc perpendicular 0.5 s	APM parallel/Arc perpendicular 0.5 s	Arc parallel, 0.6 s	(Levin et al. 2004)
Hokkaido	Arc parallel, 0.1 s	Arc perpendicular, 0.3 s	Arc perpendicular, 0.3 s	(Nakajima et al. 2006)
Honshu	Arc parallel, 0.1 s	APM parallel/Arc perpendicular 0.3 s	APM parallel/Arc pependicular, 0.3 s	(Nakajima & Haswagawa 2004)
Ryukyu		Arc parallel, 1.0 s		(Long & van der Hilst 2006)
Izu-Bonin		Arc parallel, 1.2 s		(Anglin & Fouch 2005)
Mariana	Arc parallel, 0.5 s	Arc parallel, 0.5 s	APM parallel beyond spreading center, 0.6 s	(Pozgay et al. 2007a)
Tonga	Arc parallel	Arc parallel, 1.5 s	APM parallel/Arc perpendicular beyond spreading center, 1 s	(Smith et al. 2001)
Hikurangi (New Zealand)	Arc parallel, 0.5 s	Variable, 1 s	Variable, 1 s	(Audoine et al. 2004)
Cascadia	APM parallel, 0.8 s	APM parallel, 1.2 s	APM parallel, 1.2 s	(Currie et al. 2004)
Central America	Arc parallel, 0.2 s	Arc parallel, 0.5 s		(Abt et al. 2006)
Chile	Variable	Slab contour parallel, 0.2 s	Slab contour parallel, 0.3 s	(Anderson et al. 2004)

*Additional references given in Wiens & Smith (2003) and Lassak et al. (2006).
Absolute plate motion of the subducting plate (APM).

the forearc and arc, but fast directions also rotate to convergence parallel near the backarc spreading center (Pozgay et al. 2007a). In the Japanese arc, this rotation occurs between the forearc and volcanic arc, such that measurements beneath the volcanic arc and backarc show arc-perpendicular orientations (Nakajima & Hasagawa 2004, Long & Van der Hilst 2005, Nakajima et al. 2006).

3. INTERPRETATION OF SEISMIC RESULTS

3.1. Variables Affecting Seismic Velocity and Attenuation

As outlined above, seismic observations of subduction zones show large variations, ranging from fast velocity and low attenuation in slabs to slow velocity and high attenuation in the mantle wedge, with significant and variable seismic anisotropy. Seismic observations can potentially be affected by a large range of variables, including temperature, composition, volatile content, and the presence of small quantities of melt or other fluids. Distinguishing between the effects of these parameters is

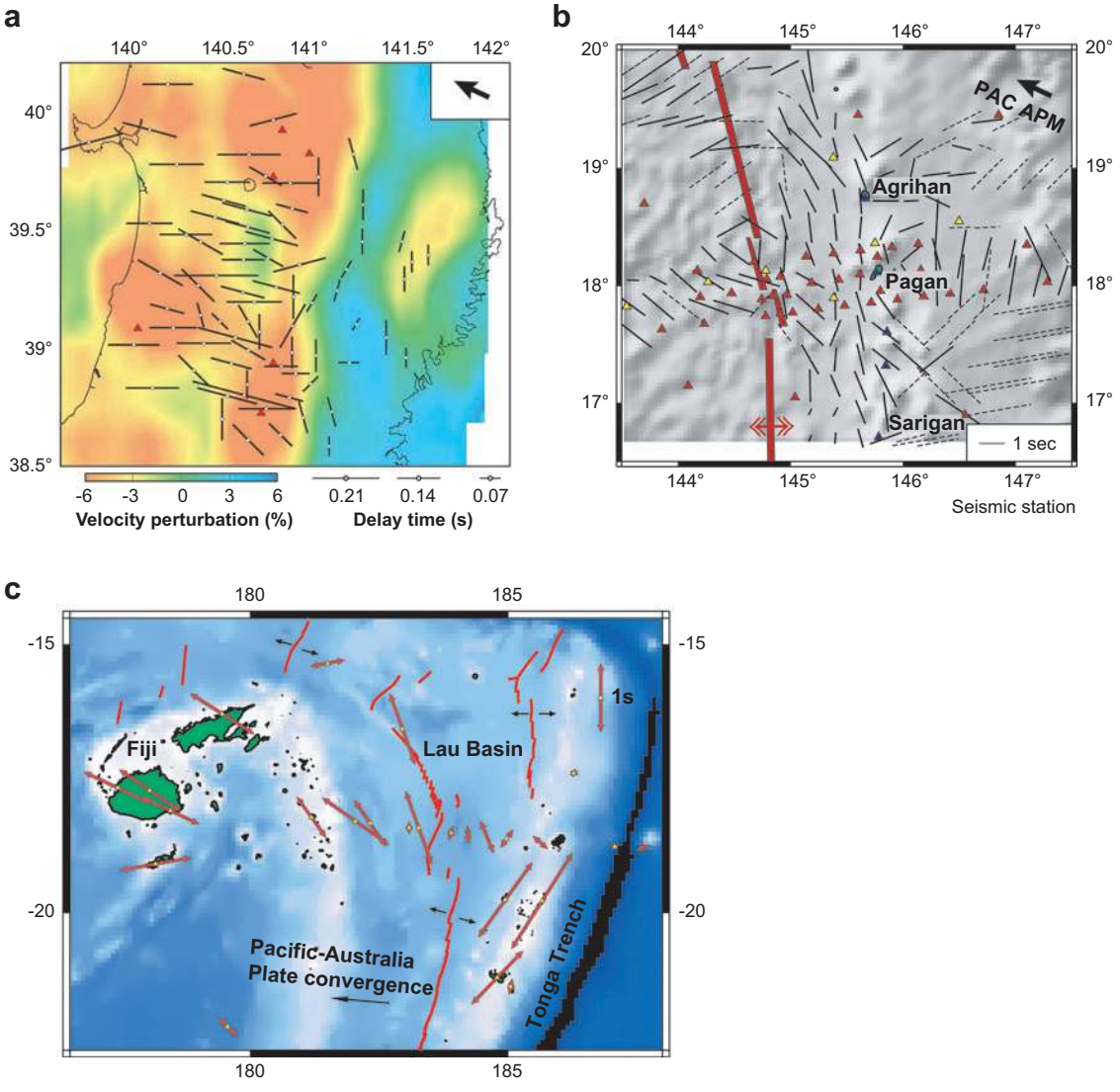

Figure 4

Shear wave splitting observations showing the directions of the fast polarization axis for near-vertically propagating S waves at three subduction zones. (*a*) The northeast Japan subduction zone (Nakajima & Hasagawa 2004), (*b*) the central Mariana subduction zone (Pozgay et al. 2007a), (*c*) the Tonga-Lau subduction zone (Smith et al. 2001). In all three cases, along-strike fast directions predominate in the forearc. For the Japan case, the fast directions rotate to arc-normal beneath the volcanic arc, whereas for the Mariana and Tonga cases, the rotation occurs in the far backarc, beyond the backarc spreading center.

essential if the seismic images are to provide quantitative constraints on geodynamic processes. In this section, we review a range of conditions that will affect seismic properties, starting with thermally activated processes. In Section 3.3, the experimental observations and theoretical models are compared to the seismic observations and geodynamic models discussed in Section 3.2.

3.1.1. Thermally activated processes. At low temperatures the behavior of rocks at seismic frequencies is purely elastic, with a linear decrease of the elastic moduli with increasing temperature (anharmonic behavior). Elastic properties are most commonly determined by experiments at ultrasonic frequencies (e.g., Anderson & Isaak 1995, see also references in Schutt & Lesher 2006). In the elastic regime, the response of a material to an imposed stress occurs instantaneously and without energy loss (zero attenuation or infinite Q). At higher temperatures, rocks respond viscoelastically to the imposed stress, where energy absorption (finite Q) and corresponding dispersion (frequency dependence of wave velocities) become progressively more important (Berkhemer et al. 1982; Jackson et al. 1992, 2002; Gribb & Cooper 1998). For olivine the transition from elastic to viscoelastic behavior occurs at about 950°C at seismic frequencies (Faul & Jackson 2005). Seismic attenuation increases rapidly with temperature above 950°C and anelastic velocity dispersion becomes more important for interpreting seismic velocities at higher temperatures (e.g., Karato 1993).

Fits to subresonant (torsional) data, as well as microcreep experiments, confirm that the observed strain consists of elastic (instantaneous and recoverable), anelastic (transient and recoverable), and viscous (permanent time-dependent) contributions. The experimental data can be fit by two alternative empirical models that account for these three parts: the Andrade (e.g., Gribb & Cooper 1998) and Burgers models (e.g., Faul & Jackson 2005). The Burgers model has to be extended to produce a distribution of relaxation times implicit in the seismically observed absorption band behavior (Minster & Anderson 1981). The moduli measured on polycrystalline samples in the viscoelastic regime at seismic frequencies (1–1000 s) are strongly and nonlinearly temperature as well as grain-size dependent (**Figure 5**) (Jackson et al. 2002, Faul & Jackson 2005).

A number of physical processes can give rise to recoverable, but time- and temperature-dependent (anelastic) strains imposed by the seismic wave field: the motion of point defects, line defects (dislocations), and planar defects (grain boundaries, twins). Models of point defects indicate that the anelastic relaxation occurs at much higher frequencies than the seismic band (i.e., point defects do not contribute to seismically observed attenuation), and the associated modulus reduction is small (Karato & Spetzler 1990).

Hydrogen-related defects are an exception, as water in nominally anhydrous minerals can have a large effect on seismic velocities and attenuation (Karato 2003, Shito et al. 2006). Water (hydrogen) does not affect the anharmonic moduli, but may enhance processes that are also temperature dependent, such as dislocation climb and grain boundary sliding. The influence of water on anelastic behavior is inferred from its effect on viscous behavior determined by conventional deformation experiments (e.g., Mei & Kohlstedt 2000a,b).

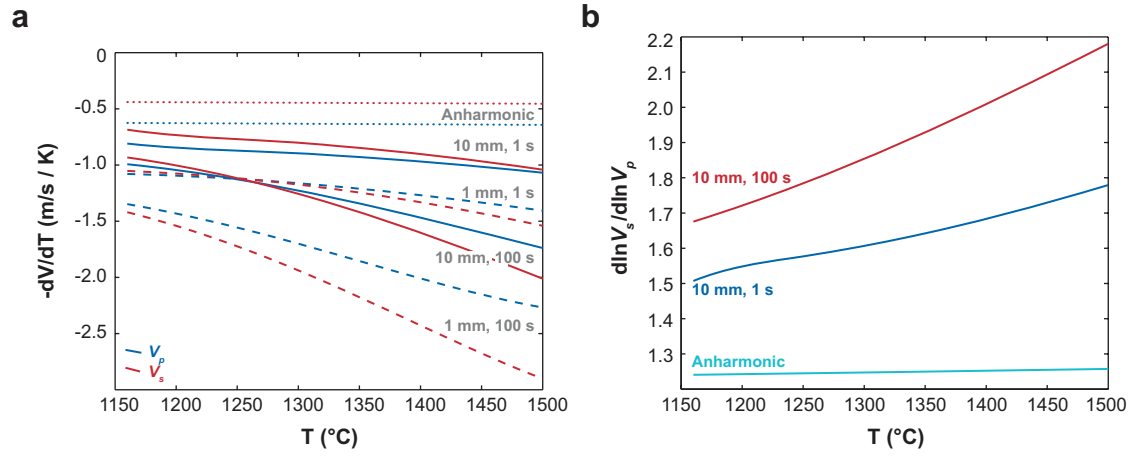

Figure 5

(*a*) P-wave (*blue*) and S-wave (*red*) velocity temperature derivatives as a function of temperature for periods of 1 and 100 s and grain sizes of 1 and 10 mm at 100 km depth. Solid lines denote 10 mm grain size, dashed lines denote 1 mm grain size, and dotted lines denote anharmonic results that are independent of grain size. The shear modulus is calculated from the fit of Faul & Jackson (2005) to the experimental data of Jackson et al. (2002, 2004). Anharmonic values and derivatives for bulk and shear modulus are taken from Bass (1995). These calculations assume that there is no viscoelastic relaxation of the bulk modulus (no bulk attenuation). Temperature derivatives accounting for viscoelastic behavior of the shear modulus are nonlinear and are substantially larger at high temperatures than the anharmonic velocity derivatives. (*b*) The logarithmic ratio $d\ln V_s/d\ln V_p$ as a function of temperature for a grain size of 10 mm and periods of 1 s and 100 s, using the same methods as panel *a*. The ratio is calculated from $d\ln V_s/d\ln V_p = (V_p/V_s)[(dV_s/dT)/(dV_p/dT)]$, where V_i are the anharmonic velocities at temperature T and dV_i/dT are the temperature derivatives at temperature T from panel *a* (see Karato 1993). These calculations show that logarithmic ratios as high as 2 can result from temperature effects alone (cf. Section 2.1).

Mantle anisotropy is generally associated with deformation by dislocation creep, indicating that dislocations have the potential to affect the seismic properties. Microphysical models of dislocation damping show that the shear modulus decrease due to interaction of dislocations with the seismic wavefield may be large (Karato & Spetzler 1991, Jackson 2007). However, a number of conditions have to be met regarding activation energy, dislocation segment length distributions, and densities to produce the seismologically observed absorption band behavior. In the only experimental study to date, Gueguen et al. (1989) observed a significant increase in attenuation from undeformed to predeformed single crystals of olivine, but the results are not conclusive.

Grain sizes in the upper mantle are estimated to lie in the millimeter to centimeter range, implying that grain boundaries are a ubiquitous defect. Grain boundaries are assumed to have significantly lower viscosities than grain interiors (e.g., Raj & Ashby 1971; see also Section 3.1.3), an assumption that is also made in the description of diffusional creep accommodated by grain boundary sliding (Poirier 1985, Hirth & Kohlstedt 1995). High-resolution images of polycrystalline olivine show grain

boundary regions of approximately 1 nm or less in width that do not have olivine structure and are enriched in trace elements relative to grain interiors (e.g., Drury & FitzGerald 1998, Hiraga et al. 2003, Faul et al. 2004).

Diffusionally accommodated grain boundary sliding involves a monotonic distribution of relaxation times. This distribution of thermally activated relaxation times provides a natural explanation for the "high temperature background" or absorption band behavior. As indicated in Section 2.2, the experimentally determined frequency dependence of attenuation associated with this process, $Q \sim (\omega d)^{\alpha}$ where ω is the frequency, d grain size, and $\alpha \approx 0.26$ (Jackson et al. 2002) is consistent with the seismologically determined frequency dependence. The temperature derivatives of the velocity in **Figure 5** include the corresponding frequency and grain-size dependence of the shear modulus. At high temperatures velocity derivatives including anelasticity are twice as large as anharmonic derivatives at body wave frequencies and a grain size of 10 mm. At the same conditions, the V_p/V_s ratio can exceed 1.8.

In summary, temperature is expected to have a significant effect on seismic velocities and attenuation via processes such as grain boundary sliding and dislocation damping. The temperature effects become progressively more prominent as temperature increases, and are not well approximated by linear temperature derivatives often assumed in the seismological literature (**Figure 5**). Because of the expected large temperature differences between subducting lithosphere and mantle wedge, the contribution of temperature to observed velocities should be accounted for first to identify contributions from other factors such as melt or water.

3.1.2. Composition. Variations in seismic velocities owing to compositional changes in upper mantle rocks can result from changes in either the composition of constituent minerals (for example, the Fe content of olivine) or changes in mode (changes in the proportion of the constituent minerals in a rock). Two different processes can result in compositional changes: partial melting and melt extraction, or metasomatic infiltration of a host rock by melts of fluids.

Jordan (1979) and Schutt & Lesher (2006) examined the effects of progressive depletion on seismic velocities and densities by melt extraction from a model fertile mantle composition. Melt extraction depletes principally the low melting point components such as Fe and Al. As a result, olivine and pyroxenes become more magnesian and, hence, less dense and seismically faster. A decrease in Al content of the bulk rock results in a decrease of the proportion of garnet (or spinel at pressures below 2-3 GPa), which again reduces the density of the bulk rock. However, because garnet has faster seismic velocities than olivine and pyroxenes, a decreasing garnet mode decreases bulk rock seismic velocities. Metasomatized xenoliths show a wider range in composition (Lee 2003), but for the full range in Mg# (from 89 to 93) the range in shear velocities is approximately 0.1 km s^{-1} at standard pressure and temperature. Compared to temperature variation or the presence of melt, which give rise to viscoelastic behavior, compositional variations of a (dry) peridotitic upper mantle at temperatures above about 1000°C will be difficult to detect in a subduction zone setting.

For ultramafic compositions in the upper mantle, only two minerals are potentially abundant enough to lower velocities by more than 0.1 km s^{-1}: plagioclase and amphibole. From calculations by Stixrude & Lithgow-Bertelloni (2005), the presence of plagioclase may in part explain the observations of a near constant velocity lid for oceanic lithosphere by reducing the shear velocity in the upper 20–30 km (the stability limit of plagioclase). Amphibole is significantly slower than dry peridotite minerals (Hacker et al. 2003). The stability of (pargasitic) amphibole in a peridotitic composition is restricted to pressures below 3 GPa and temperatures below 1000°C (e.g., Niida & Green 1999). Thus amphibole can produce significantly lower velocities but only in the shallower (<100 km) and cooler parts of the mantle wedge.

Serpentinization of the forearc mantle is often invoked to explain the disappearance of the seismic Moho in subduction settings (e.g., Hyndman & Peacock 2003; see Sections 2.1 and 3.2.1). Using the data compiled by Hacker et al. (2003), for serpentinized harzburgite to have similar velocities (and densities) as (anhydrous) mafic lower crustal lithologies, the degree of serpentinization needs to be close to 30%. Because of the low shear modulus relative to the bulk modulus of serpentine (antigorite), a diagnostic feature of serpentinized harzburgite in seismic images is a large V_p/V_s ratio.

3.1.3. Melt and fluids. Melt and fluid, ranging in composition from volatile-free silicate melt to nearly pure H_2O/CO_2 fluids, have a lower bulk modulus than crystalline solids (e.g., Rivers & Carmichael 1987) and no elastic resistance to shear. Their distribution in the solid matrix is controlled by surface energy such that even for a small proportion they are optimally dispersed among crystalline grains to impact bulk properties [i.e., for a dihedral angle (θ) with $0 < \theta < 60°$, fluid occurs at every three-grain edge intersection]. Small amounts of melt or fluid can therefore have a large effect on seismic velocities and attenuation.

Two different theoretical methods, the self-consistent scheme and poroelastic theory, are commonly used to determine the effect of a distributed weaker phase on the bulk properties of rocks. In the self-consistent scheme, the effect of a pore with a specified geometry is determined by replacing the elastic moduli of the pore-free medium with effective elastic moduli that account for the mechanical interaction of the pores (e.g., O'Connell & Budiansky 1974, 1977; Mavko 1980; Schmeling 1985). Pore shapes are approximated by prescribed geometries such as circular cracks or ellipsoids (O'Connell & Budiansky 1974, 1977; Schmeling 1985) or tubules (Mavko 1980). Poroelastic theory is based on a continuum mechanical approach for two-phase media to determine the elastic properties of a matrix skeleton where the pore fluid is replaced by a vacuum (e.g., Biot 1956; Takei 1998, 2002; Berryman 2000). Local heterogeneities in the pore space or viscous shear within the fluid are not considered in this approach (Schmeling 1985).

In the poroelastic approach developed by Takei (1998, 2002), the proportion of grain to grain contact area (contiguity) of a porous skeleton determines the mechanical properties of the composite. Depending on the method, modulus reduction and attenuation are then calculated as a function of crack density, porosity, or contiguity.

The self-consistent scheme describes three distinct processes resulting in modulus reduction and attenuation (O'Connell & Budiansky 1977). On application of a macroscopic stress, shear stress relaxation in the fluid or melt within individual inclusions (e.g., between opposite faces of a sheared inclusion) occurs first. This process is equivalent to elastically accommodated grain boundary sliding (discussed in Section 3.1.1). Second, flow within or between connected inclusions with different orientations to the applied stress takes place, and third, if the fluid is interconnected, bulk fluid flow can occur. Completion of the first two processes results in shear modulus reduction relative to a melt-free aggregate, but the bulk modulus remains unaffected. Completion of the third process results in bulk modulus reduction, but the shear modulus is unaffected (O'Connell & Budiansky 1977).

Seismic attenuation only occurs if the relaxation timescale of a particular process, i.e., the transition from unrelaxed (at higher frequencies) to relaxed modulus (at lower frequencies), falls in the seismic frequency band. For upper mantle fluids and melts, the relaxation due to the first process takes place at much higher frequencies than the seismic band and therefore no attenuation is observable at seismic frequencies (O'Connell & Budiansky 1977, Mavko 1980). Similarly, relaxation via the second mechanism [termed melt squirt by Mavko & Nur (1975)] is also estimated to take place at frequencies higher than seismic frequencies (Hammond & Humphries 2000, Faul et al. 2004). Completion of both processes results in a reduced shear modulus in the seismic band relative to melt-free mantle, or in other words, a reduction of seismic velocity with no corresponding increase in seismic attenuation.

The relaxation timescale of the third mechanism, bulk fluid flow, is less clear. Renner et al. (2003) inferred that the basaltic melt compaction rate is limited by the flow of melt out of the sample at experimental durations of 6 h. Gribb et al. (1994, see also Cooper 2003) inferred that transient (anelastic) behavior observed in four-point-bending experiments was at least partially due to bulk melt flow across the specimen. The timescale of the observed transients was of the order of tens of seconds to hours. Extrapolation to partially molten regions in the mantle requires extrapolation of the experimentally observed behavior to mantle grain sizes and the pressure gradients of the seismic wavefield. Significantly, poroelastic theory explicitly assumes that relaxation by bulk fluid flow has taken place (e.g., Takei 1998, 2000, 2002).

Experimental observations on partially molten olivine within the seismic frequency band show an attenuation peak owing to melt, superposed on a monotonic background similar to melt-free samples (Jackson et al. 2004). These observations can most easily be reconciled by inferring grain boundary sliding as the mechanism responsible for modulus reduction and attenuation (Faul et al. 2004). If this mechanism has been correctly identified, the theoretical treatments of Raj & Ashby (1971) and O'Connell & Budiansky (1977) imply that the grain boundary viscosity is intermediate between that of bulk melt and olivine grain interiors. Velocity reduction and attenuation in melt-free samples is due to diffusionally accommodated grain boundary sliding, and the attenuation peak in the melt-bearing results is consistent with elastically accommodated grain boundary sliding, implying grain boundary viscosities in the range of 10^4–10^9 Pa s. Extrapolation of the experimental results to mantle grain sizes indicates that the broad attenuation peak falls in the seismic frequency range

for upper mantle temperatures and grain sizes (Faul et al. 2004). This could lead to variable frequency dependence if a broad enough frequency range is investigated and in situ melt fractions are high enough. The attenuation peak within the seismic band results in large attenuation for relatively small (~0.1%) porosity, suggesting that attenuation will be highly sensitive to even small melt fractions (Faul & Jackson 2004).

In summary, theoretical treatments as well as experimental observations predict that melt will significantly reduce seismic velocities (depending on melt fraction and pore geometry), whereas only the experimental observations suggest observable melt-related attenuation. However, quantification of melt porosity in the mantle by seismic observations remains difficult at this time.

3.2. Insights from Geodynamical Modeling

Many geological processes occurring in the mantle wedge have been examined through geodynamic models, including the evolving thermal structure, melt generation and transport behaviors, and mantle flow patterns. In a typical model formulation, the downgoing slab, overriding plate, and mantle wedge asthenosphere are usually explicitly defined, whereas the forearc, arc, and backarc must be inferred from the model results.

3.2.1. Cold forearc wedge/decoupling zone. Despite being relatively cold and amagmatic, the forearc plays a crucial role in arc evolution. As the forearc is the portion of the overlying plate that is directly on top of the subducting slab and close to the trench, the forearc experiences high stresses (Kneller et al. 2005), can be significantly hydrated and serpentinized (Fryer et al. 1995, Hyndman & Peacock 2003), and is susceptible to internal deformation and faulting. Forearc deformation occurs at dramatically different P-T (and rheological) conditions and at much slower strain rates than in the rest of the mantle wedge, so geodynamic models are rarely designed to simultaneously address wedge flow and forearc deformation. Because corner flow is driven by the viscous coupling between slab and overlying mantle, the fault zone parameterization affects the mode of coupling and flow pattern in the uppermost wedge. Thus, exactly how the viscous decoupling is achieved along the fault zone separating the downgoing slab from the overriding forearc can be crucial to the results of the model. Fault zone dimensions may be set to some a priori depth or can be defined by some other criterion, such as yield strength (Zhong & Gurnis 1995, Conder 2005). Computer codes that can realistically handle rapidly varying viscoelastic-plastic rheologies will help address the coupling and simultaneous deformation within the forearc corner and asthenospheric wedge (Hall et al. 2003), but they remain computationally expensive.

For wedge models focused on asthenosphere dynamics, the few strong constraints on the proper fault zone dimensions for viscous flow models and subsequent forearc development are mentioned above in Section 2.1, including the transition from low to high heatflow and seismic attenuation from the forearc to toward the arc. These constraints point to a decoupling depth between 60–80 km (Conder 2005, Furukawa

1993) and a forearc-asthenosphere boundary that is fairly abrupt, vertical, and a few tens of kilometers oceanward of the volcanic front. This depth is greater than the maximum depth of thrust seismicity for most arcs (Tichelaar & Ruff 1993), but the lower part of the decoupling zone may fail during slow slip events that have been detected both geodetically and seismically (e.g., Rogers & Dragert 2003, Ito et al. 2007). A useful rule for viscous flow thermal models is that the deeper the viscously decoupled fault zone extends, the less viscous erosion of the upper plate and the warmer slab surface temperatures become by sequestering more cold material in the forearc corner, restricting the amount of possible cold material creating a cool thermal blanket atop the slab. Consequently, the depth of the forearc corner controls the depth of viscous coupling, which controls asthenospheric penetration and flow in the corner, affecting slab heating and melt processes in the wedge corner (Conder 2005).

3.2.2. Asthenospheric flow. Mantle flow in the wedge has important implications for the thermal structure, arc melting processes and general mantle circulation. The majority of mantle wedge flow models in the literature assume a 2D corner flow structure within the wedge for a variety of reasons. Two-dimensional models are simpler to construct and interpret, and unless there is specific interest in slab edges or tears, a case may be made that near the center of slabs most processes should be largely 2D. However, there is some evidence that 3D mantle flow may be common beneath arcs, and should be considered in interpretation of the spectrum of geological and geophysical observations.

As described above in Section 2.4, mantle minerals are anisotropic and align themselves in the presence of a strain field (Mainprice & Silver 1993), so observations of seismic anisotropy provide important constraints on mantle flow in the wedge. Observed patterns need to be interpreted cautiously, as mineral textures may develop with differing fast axis orientations relative to the flow direction as a result of melt band formation (Holtzman et al. 2003) or under conditions of hydration and high stress (Jung & Karato 2001, Katayama & Karato 2006). The forearc is likely a region of low temperatures, high water content, and high stress and may be dominated by B-type fabric, which exhibits seismic fast directions normal to the maximum extension direction, whereas the wedge asthenosphere supports mineral fabrics which give seismic fast directions orientated in the flow direction for vertically traveling S-waves (Kneller et al. 2005, Katayama & Karato 2006).

Fast splitting orientations in the Lau and Mariana mantle wedges are arc-parallel in the forearc and beneath the arc, but rotate toward arc-perpendicular (or parallel to the apparent plate motion of the subducting plate) further into the backarc (Smith et al. 2001, Pozgay et al. 2007a) (**Figure 4** and **Table 1**). In neither case are the observations consistent with simple 2D slab-driven flow as is assumed in many geodynamic models (e.g., Ribe 1989, Fischer et al. 2000, Conder 2002) and instead imply more complex patterns of mantle flow. Geodynamic models using analog materials demonstrate that flow around the ends of slabs and along-strike in the mantle wedge can dominate systems characterized by slab rollback (Buttles & Olson 1998, Kincaid & Griffiths 2003).

Recent advances in 2.5-dimensional (2.5D) and 3D numerical modeling are helping to address the causes and effects of along-axis flow (Conder et al. 2006, Kneller

& van Keken 2006). While 3D modeling is required to fully integrate all the interrelated dynamics, 2.5D flow models (flow is allowed in the along-arc direction, but with no variation) can be used for looking at specific processes required for the development of seismic anisotropy by lattice-preferred orientation (LPO) of anisotropic mantle minerals in the presence of along-arc flow. For example, taking a 2D thermal model with non-Newtonian rheology and calculating the flow and strain rates in the along-strike direction under an applied along-strike pressure gradient, one finds along-strike flow velocities are greatest beneath the arc, resulting in high strain rate localizations at the base of the overlying plate beneath the arc and backarc, and atop the inclined slab (Pozgay et al. 2007a). It is likely that observed shear wave splitting patterns would be dominated by the signatures of these loci of high stain rates in wedge systems with a high degree of arc-parallel mantle flow. Similarly, 2.5D flow models coupled with LPO development under strain (Kaminski et al. 2004) patterned after the Lau Basin, suggest that mantle velocities several times the plate velocities and confined to a low-viscosity subarc channel (Billen & Gurnis 2001) are required to explain the observed shear wave splitting pattern (**Figure 6)** (Conder & Wiens 2007).

Even barring along-strike flow, simple 2D corner flow may not adequately describe mantle flow within the wedge. The complete role of gravitational instabilities in the wedge is difficult to constrain, but may be key to a number of important aspects of wedge dynamics. Buoyant diapirism could play crucial roles in fluid and melt transport, possibly controlling ascent times, distribution throughout the wedge, and location of the volcanic front (Gerya et al. 2004, Hall & Kincaid 2001). Hot fingers in the wedge beneath Japan suggest that small-scale convection may strongly affect wedge corner structure and volcano distribution (Tamura et al. 2002, Nakajima et al. 2001). The negatively buoyant instabilities from the base of the overlying plate driving small-scale convection are likely time dependent and may control the migration of active volcanism across the arc (Honda et al. 2002).

3.2.3. Melt generation. Melt generation has been a focus of geodynamic subduction models nearly since the inception of plate tectonics. Melting beneath arcs can result from several possible processes: hydration (flux) melting of the wedge from the release of slab fluids (Tatsumi 1989), decompression melting of the wedge due to upwelling flow (Conder et al. 2002), or melting of the downgoing sediments and/or basaltic crust (Hsui et al. 1983). More than one mechanism may occur simultaneously beneath any particular arc (**Figure 7**). Flux melting is widely viewed as the primary mechanism of arc magmagenesis (e.g., Iwamori, 1998, van Keken 2003), but because of complexities in fluid release, migration, and solid-fluid interaction, quantitative models of the system including processes from slab fluid release to fluid migration and subsequent melting are few. Slab melting is a simpler process but has often been discounted at arcs except in unusual tectonic settings, largely because some thermal models showed that the slab crust is likely to be too cold to melt within the depth range required to generate arc volcanoes (Davies & Stevenson 1992, Peacock et al. 1994). However, geochemical studies suggest a signature of slab sediments in arc magmas (Johnson & Plank 1999) and recent modeling results using temperature-dependent viscosity suggest the possibility that slab melting contributes a volumetrically small

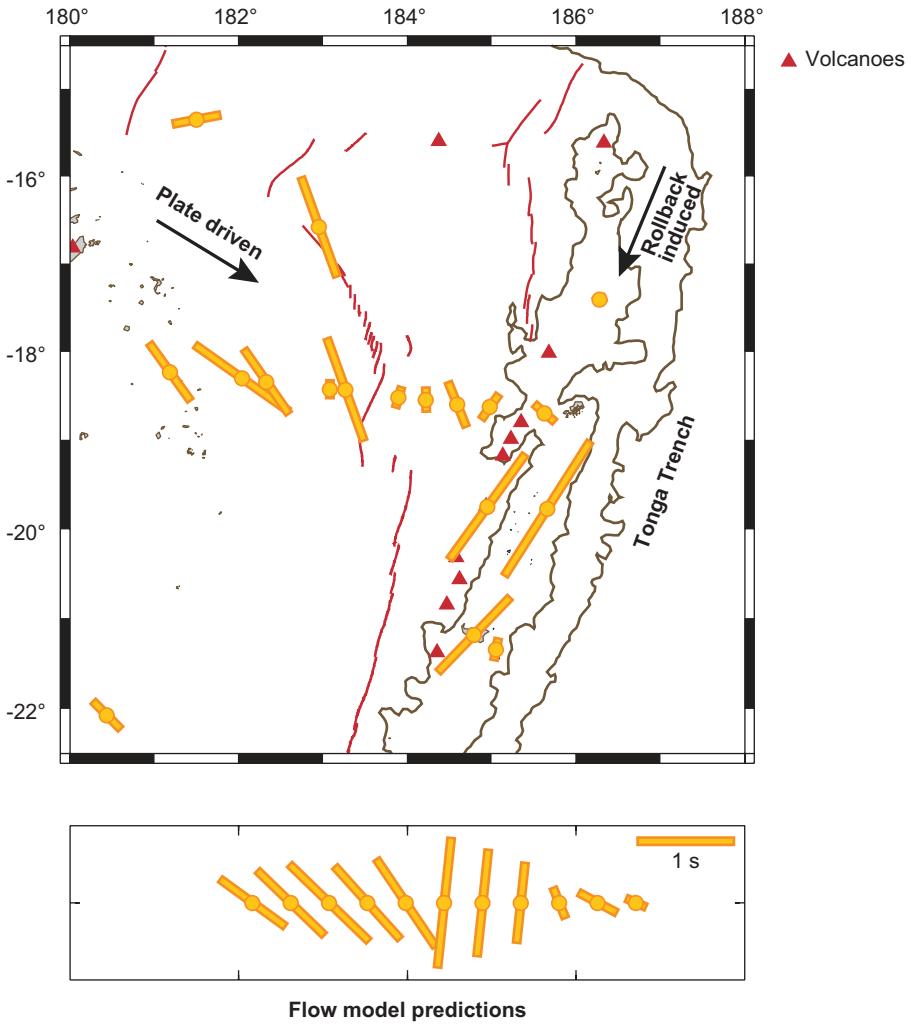

Figure 6

Three-dimensional flow may be an essential aspect of arc dynamics. Top panel shows stacked shear wave splitting results of Smith et al. (2001) for the Lau Basin from local S phases. Bars denote seismic fast directions with lengths scaled to splitting times. The shear wave splitting observations are likely controlled by mantle flow patterns. Bottom panel shows predicted shear wave splitting for vertically traveling waves through the wedge using 2.5D wedge flow modeling that includes both corner flow and along-strike flow while tracking LPO development. A model with channelized flow along the arc likely induced from slab rollback results in fast directions controlled by corner flow in the backarc, and along-strike flow beneath the arc, producing a good match to the observed splitting data (Conder & Wiens 2007).

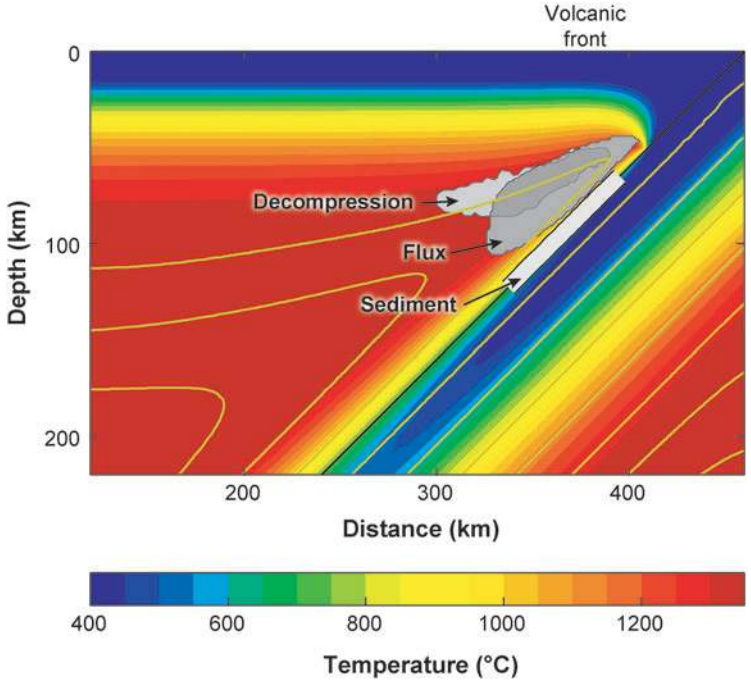

Figure 7

Melting at volcanic arcs can be induced through three possible mechanisms: fluxing of the wedge from hydrous fluids, decompression melting with lithospheric ablation, and melting of the top of the slab at depth. The expected regions of decompression, flux, and slab/sediment melting (*gray fields*) are shown as determined using the idealized arc flow model of Conder (2005) (slab dip of 45, subduction rate of 6 cm year^{-1}, temperature-dependent viscosity) and including the hydration saturation and wet solidus parameterization of Katz (2002). VF denotes the volcanic front, assumed to be where the slab reaches 100 km depth, and colors denote temperatures calculated in the flow model.

but geochemically significant component to arc magmatism (Kelemen et al. 2003, Conder 2005).

Despite petrological and geochemical evidences of anhydrous melting of the wedge at arcs (Cameron et al. 2003, Elkins-Tanton et al. 2001, Sisson & Bronto 1998), decompression melting has often been overlooked because significant upwelling only occurs in models that explicitly include a realistic temperature-dependent viscosity (Furukawa 1993, Eberle et al. 2002, Conder et al. 2002). Each melting mechanism exhibits a different spatial pattern of melt generation, suggesting the prospect of distinguishing between the probable melting processes at arcs through geophysical imaging (**Figure 7**). However, there are a number of poorly understood processes and conditions that will make interpretation difficult using geophysical imaging alone. Seismic anomalies depend on temperature, composition, and the presence of melt and fluids (Wiens et al. 2006b; see also Section 3.1). So, the geophysical anomalies will depend strongly on the migration patterns of melt and fluids in conjunction with pore

geometry, which are presently not well constrained. Such ambiguity demonstrates the importance of building a consistent model using geochemistry, geophysical imaging, and geodynamical modeling.

3.2.4. Fluid/melt migration. Although it is well understood that the slab releases volatiles into the mantle wedge, there is some uncertainty as to the most crucial dehydration reactions and transport mechanisms governing the process (van Keken 2003). The governing reactions could vary between different arcs as they are functions of T, P, and mineral content and composition. Models of punctuated pulses of fluid release associated with pressure-dependent dehydration reactions (Tatsumi 1989) are attractive in that they easily explain the location and narrow width of the volcanic zone. However, models of slab dehydration occurring over an extended depth range fit laboratory constraints better (Ono 1998, Schmidt & Poli 1998), and require some lateral migration, in addition to buoyancy, for fluids and/or melts.

The ability of fluids and melt to migrate by porous flow depends on interconnection and geometry of the pore space. Although silicate melts are interconnected at all melt fractions [dihedral angle $<60^\circ$ (Waff & Bulau 1979)], water and CO_2-rich fluids only become interconnected at small porosity for high enough pressures (Mibe et al. 1999), at which the miscibility gap between hydrous fluids and silicate melts closes (Bureau & Kepler 1999). For interconnected fluids and melts, the permeability k is commonly calculated from $k = d^2 \Phi^n / C$, where d is the channel spacing (grain size), f is porosity with exponent n, and C a constant. From analogue permeability measurements of Wark & Watson (1998, see also Liang et al. 2001), $n = 3$ and $C = 270$. Owing to their much lower viscosity and lower density relative to silicate melts, aqueous fluids can migrate at much lower porosity (Faul 2001). Cagnioncle et al. (2007) show that for a likely range of reasonable mantle permeabilities, the grain size must be $\geq$1 mm to allow fluids to rise fast enough to escape being carried to depth in the corner flow circulation.

Seismic imaging is most sensitive to porosity, but pore geometry is also important (see Section 3.1.3). Owing to the greater mobility and hence lower porosity of fluids relative to silicate melts, the latter may be easier to detect. Because permeability depends on porosity (see equation above), constraints on porosity would indirectly also provide constraints on permeability if the grain size is known.

Some alternative mechanisms have been hypothesized that do not rely on fast porous flow, such as hydrofracture within the wedge (Davies 1999) and the development of buoyant, cold, wet, diapirs (Gerya et al. 2004). Regardless of the mechanism for fluid transport in the wedge, some fluids must be transported rapidly into the corner to generate melting. As melting depends on the potential of water to react with the solid matrix, the assumption of rapid water transport in the wedge may be used to explore the likely region of hydration melting in the wedge. For example, using a saturation formulation for olivine (Katz 2002) the potential solubility of water for an idealized thermal flow model and resultant region of hydration melting can be calculated (**Figure 7**), with the caveat that slower transport will restrict melting to regions closer to the slab.

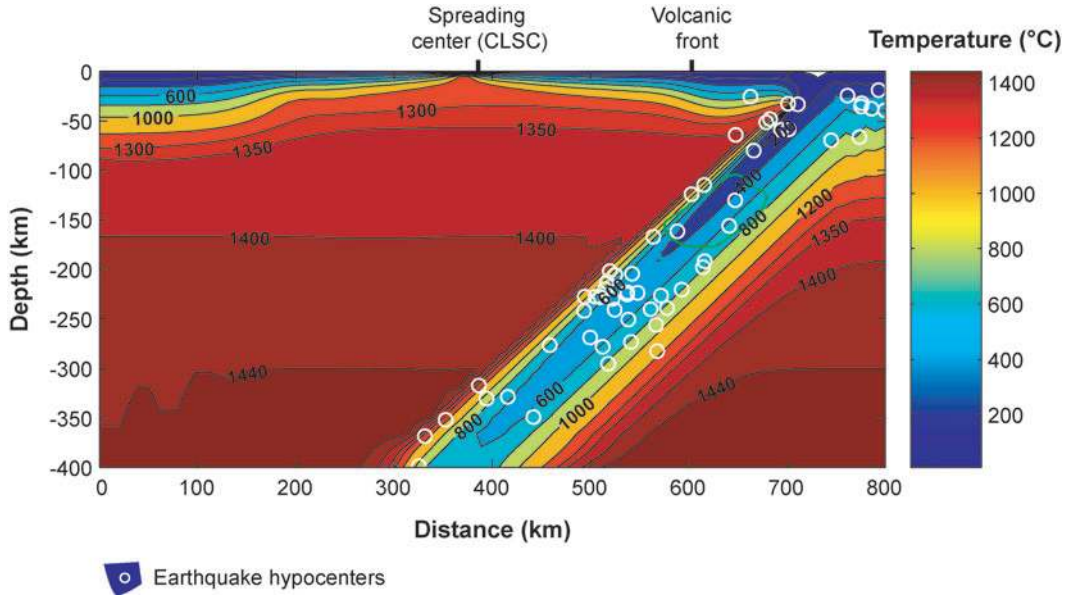

Figure 8

Temperature model calculated with methods described in **Figure 7**, using a convergence velocity and plate age appropriate for the Tonga subduction zone and including a backarc spreading center. An adiabatic temperature gradient with a potential temperature of 1350°C is included. This thermal model was used to calculate the seismic velocity and attenuation models in **Figure 9**.

3.3. Comparison to Observed Seismic Structure

The experimentally measured seismic properties of polycrystalline olivine enable forward modeling of seismic velocities and attenuation for temperature fields generated by geodynamical models (**Figure 8**). This process should allow testing and validation of geodynamical models with seismic data. Here we illustrate this procedure for the P, S, and *Q* tomographic results obtained for the Tonga arc and Lau backarc basin in Section 2 and the geodynamical models incorporating backarc spreading shown in Section 3.2.

The geodynamic model assumes an adiabatic gradient with a 1350°C potential temperature. Grain sizes in the seismic property calculations are fixed by comparison with a 1D average Pacific velocity structure (Gaherty et al. 1996, Nishimura & Forsyth 1989; see Faul & Jackson 2005). We calculate velocities and attenuation at a frequency of 1 Hz, which is the dominant frequency of the seismic observations (Conder & Wiens 2006). This procedure accounts for thermally activated processes except dislocations, which are experimentally unconstrained at this time (see Section 3.1.1).

In the resulting 2D velocity model, the upwelling owing to backarc spreading results in a shallow velocity minimum beneath the spreading center (**Figure 9**). In the

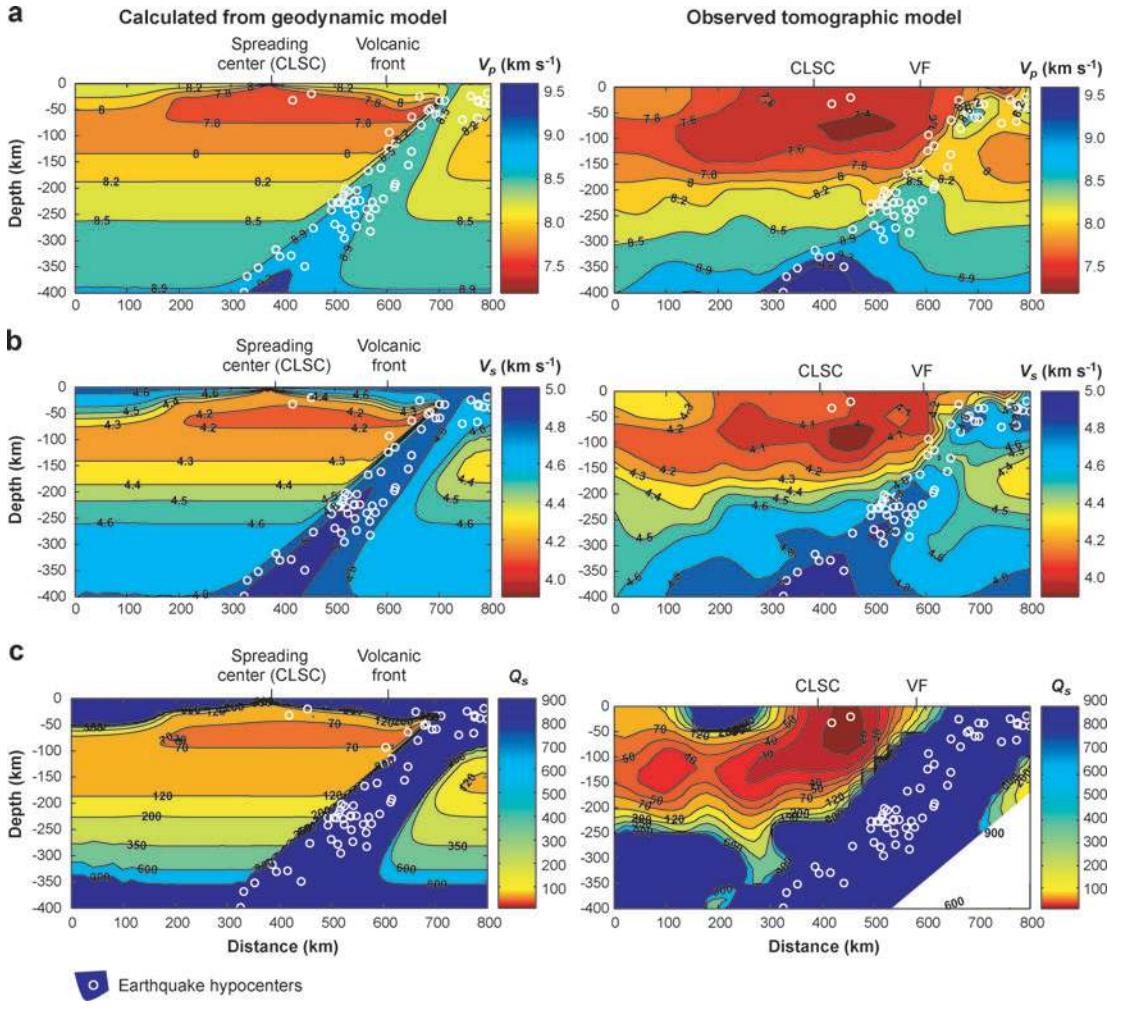

Figure 9

Forward modeling of seismic velocity and attenuation. Left side of the figure shows modeled P-wave velocity (*a*), S-wave velocity (*b*), and Q_s (*c*), using relationships given in Faul & Jackson (2005) and the temperature model shown in Figure 8. Right side shows observed tomographic velocity models for the Tonga subduction zone from Conder & Wiens (2006) and Q_s model reprocessed from Roth et al. (1999). The velocity reduction and attenuation is greater than predicted by temperature alone at depths of less than 150 km in a broad region of the Lau backarc, suggesting the additional effects of partial melt and fluids in the mantle.

slab, temperatures are generally below 900°C so that only anharmonic temperature derivatives apply. Comparison with the tomographic model of Conder & Wiens (2006) (**Figure 2**) shows that the seismically observed velocities in the wedge below approximately 200 km depth are fairly similar to the forward calculated velocities.

Above this depth, the observed velocities are significantly lower than the calculated velocities (up to 8% lower in both V_p and V_s) and extend several hundred km laterally in front of the slab. Similarly, Q is substantially lower than expected. Because the velocities below 200 km depth are well matched by the forward calculations, the low velocities above this depth do not reflect a generally hotter upper mantle adiabat. If the low velocities in the shallow upper mantle are at least in part due to high temperature, as implied by Wiens et al. (2006a), this requires a lateral inflow of mantle with elevated temperatures at this depth.

Both V_p and V_s, as well as Q, are so low that thermally activated processes alone are unlikely as an explanation for the anomaly, even if the temperature of the Lau upper mantle is greater than the average mantle. The release of water from the downgoing slab into the overlying mantle wedge suggests that water also contributes, both as defect and fluid phase, although the anomaly in **Figures 2** and **9** extends too far from the slab to be directly due to water released from the slab because basalts of the Central Lau Spreading Center do not show elevated water contents (Kelley et al. 2006).

In terms of the processes discussed in the previous sections, a combination of free fluid and melt is likely required to explain the anomalous seismic properties observed beneath the Lau basin. Observed Q is lower than expected from temperature effects alone, implying that the timescale of the relaxation process falls in the frequency range of the seismic observations. Although poroelastic theory may explain the low velocities, the implicit assumption of relaxation at frequencies above those used for the seismic observations means that it cannot explain the observed low Q. Similarly, invoking melt squirt to explain both low velocities and Q would imply either high melt viscosity or unexpectedly low aspect ratio melt inclusions, which in each case is contrary to experimental results. A process like elastically accommodated grain boundary sliding, inferred to explain the experimental observations of Jackson et al. (2004) and Faul et al. (2004), can explain both the observed Q and V_s anomalies. It is difficult to definitively infer mantle porosity from seismic observables at the present time (see Section 3.1.3), but the experimental results of Faul et al. (2004) provide a relationship between seismic attenuation and melt fraction. Interpreting **Figure 9** in terms of experimental relationships suggests that melt-free portions of the upper mantle should have $Q_s \sim 75$ at a depth of 65 km, whereas the lowest observed Q beneath the backarc is $Q_s \sim 20$. This corresponds to a melt porosity of approximately 0.1% using the results of Faul et al. (2004). Of course, the attenuation image has rather low resolution, so this does not rule out regions of higher melt porosity that are spatially too small to be resolved seismically.

Because V_p is a function of both the bulk and shear modulus, the anomalies in V_p should be milder than the anomalies in V_s if only the shear modulus is affected by anelastic processes. The seismic models from Tonga/Lau show V_p anomalies as pronounced as V_s anomalies, and the attenuation model of Roth et al. (1999) suggests a Q_p/Q_s ratio of 1.7, which is significantly different from the ratio of 2.4 predicted if attenuation is associated entirely with the shear modulus. This suggests that the bulk modulus is also affected by anelastic processes. Only one possible mechanism—bulk

fluid flow—is discussed above, although the applicability of this process remains uncertain. Inasmuch as many arc/backarc systems show substantially reduced velocities compared with global averages with simultaneous low Q (see Sections 2.2 and 2.3), similar conclusions apply.

4. CONCLUDING REMARKS

Seismic imaging methods that determine the P, S, and Q structure, as well as the anisotropic characteristics of the mantle wedge provide powerful insight into processes in the forearc, arc, and backarc. Relationships between seismic parameters and geodynamic variables such as temperature and melt content are essential for understanding the implications of the seismic observations. Experimentally derived relationships between temperature, grain size, and seismic velocity and attenuation allow us to compare geodynamic models directly with seismic observations. These results show that the observed seismic structures cannot result solely from temperature variations, and that substantial seismic anomalies are associated with melt-producing regions in the upper mantle.

This work is still in its beginning stages, as significant advances on all three fronts (seismology, rock physics, and geodynamics) will be necessary before we can quantitatively understand mantle wedge processes in detail and constrain key questions such as mantle melt porosity and the timescale of melt migration. For seismology, more detailed and higher resolution seismic models are needed. In particular, higher resolution attenuation models as well as measurements of the Q_p/Q_s ratio and the frequency dependence of attenuation, although difficult to make seismologically, will be extremely helpful in constraining the physical state of mantle materials. Detailed mapping of seismic anisotropy, including its depth dependence, is also desirable given the spatial complexity of anisotropy in the mantle wedge. Quantitative interpretation of seismic results in terms of melt porosity and water content will also require significantly better experimental constraints on their seismic effects. Finally, the application of truly 3D geodynamic models of the mantle wedge will be necessary to fully understand the complexity of mantle flow and other dynamic processes in subduction zones. We expect that substantial progress on all of these fronts in the next few years may revolutionize our understanding of processes in the mantle wedge.

DISCLOSURE STATEMENT

The authors are not aware of any biases that might be perceived as affecting the objectivity of this review.

ACKNOWLEDGMENTS

This research was supported by U.S. National Science Foundation grants OCE-0001938, OCE-0002527, and OCE-0305292, and EAR-0549056.

LITERATURE CITED

Abt DL, Fischer KM, Martin L, Abers GA, Protti JM, Gonzalez V. 2006. Shear wave splitting tomography in the Central American subduction zone: implications for flow and melt in the mantle wedge. *EOS Trans. Am. Geophys. Union* 87:T22C-05

Anderson ML, Zandt G, Triep E, Fouch M, Beck S. 2004. Anisotropy and mantle flow in the Chile-Argentina subduction zone from shear wave splitting analysis. *Geophys. Res. Lett.* 31:L23608

Anderson OL, Isaak DG. 1995. Elastic constants of mantle minerals at high temperature. In *Mineral Physics and Crystallography, A Handbook of Physical Constants*, ed. TJ Ahrens, pp. 64–97. Washington, DC: Am. Geophys. Union

Anglin DK, Fouch MJ. 2005. Seismic anisotropy in the Izu-Bonin subduction system. *Geophys. Res. Lett.* 32:L09307

Armstrong RL. 1991. The persistent myth of crustal growth. *Aust. J. Earth Sci.* 38:613–30

Audoine E, Savage MK, Gledhill K. 2004. Anisotropic structure under a back arc spreading region, the Taupo Volcanic Zone, New Zealand. *J. Geophys. Res.* 109:B11305

Barklage M, Conder J, Wiens DA, Shore P, Shiobara H, et al. 2006. 3-D seismic tomography of the Mariana mantle wedge from the 2003–2004 passive component of the Mariana Subduction Factory Imaging Experiment. *EOS Trans. Am. Geophys. Union* 87:T23C-0506

Berryman JG. 2000. Seismic velocity decrement ratios for regions of partial melt in the lower mantle. *Geophys. Res. Lett.* 27:421–24

Billen MI, Gurnis M. 2001. A low viscosity wedge in subduction zones. *Earth Planet. Sci. Lett.* 193:227–36

Biot MA. 1956. Theory of propagation of elastic waves in a fluid-saturated porous solid. 1. Low-frequency range. *J. Acoust. Soc. Am.* 28:168–78

Blakely RJ, Brocher TM, Wells RE. 2005. Subduction-zone magnetic anomalies and implications for a hydrated forearc mantle. *Geology* 33:445–48

Bostock MG, Hyndman RD, Rondenay S, Peacock SM. 2002. An inverted continental Moho and serpentinization of the forearc mantle. *Nature* 417:536–38

Brocher TM, Parsons T, Trehu AM, Snelson CM, Fisher MA. 2003. Seismic evidence for widespread serpentinized forearc upper mantle along the Cascadia margin. *Geology* 31:267–70

Brown M, Rushmer T, eds. 2006. *Evolution and Differentiation of the Continental Crust*. Cambridge, UK: Cambridge Univ. Press. 550 pp.

Bureau H, Keppler H. 1999. Complete miscibility between silicate melts and hydrous fluids in the upper mantle: experimental evidence and geochemical implications. *Earth Planet. Sci. Lett.* 165:187–96

Buttles J, Olson P. 1998. A laboratory model of subduction zone anisotropy. *Earth Planet. Sci. Lett.* 164:245–62

Cagnioncle A-M, Parmentier EM, Elkins-Tanton LT. 2007. The effect of solid flow above a subducting slab on water distribution and melting at convergent plate boundaries. *J. Geophys. Res.* 112:B09402

Cameron BI, Walker JA, Carr MJ, Patino LC, Matias O, Feigenson MD. 2003. Flux versus decompression melting at stratovolcanoes in southeastern Guatemala. *J. Volcan. Geotherm. Res.* 119:21–50

Christensen NI. 1984. The magnitude, symmetry and origin of upper mantle anisotropy based on fabric analyses of ultramafic tectonites. *Geophys. J. R. Astron. Soc.* 76:89–111

Conder JA. 2005. A case for hot slab surface temperatures in numerical viscous flow models of subduction zones with an improved fault zone parameterization. *Phys. Earth Planet. Inter.* 149:155–64

Conder JA, Wiens DA. 2006. Seismic structure beneath the Tonga arc and Lau back-arc basin determined from joint V_p, V_p/V_s tomography. *Geochem. Geophys. Geosyst.* 7:Q03018

Conder JA, Wiens DA. 2007. Rapid mantle flow beneath the Tonga volcanic arc. *Earth Planet. Sci. Lett.* 264:299–307

Conder JA, Wiens DA, Morris J. 2002. On the decompression melting structure at volcanic arcs and back-arc spreading centers. *Geophys. Res. Lett.* 29:1727

Conder JA, Wiens DA, Pozgay SH. 2006. Trench-parallel flow in the Mariana mantle wedge: comparisons of shear-wave splitting and numerical models of mantle flow. *EOS Trans. Am. Geophys. Union* 7(52):T22C-08

Cooper RF. 2003. Seismic wave attenuation: energy dissipation in viscoelastic crystalline solids. In *Plastic Deformation of Minerals and Rocks*, ed. SI Karato, H-R Wenk, *Rev. Mineral. Geochem.* 51:253–90. Chantilly, VN: Mineral. Soc. Am.

Currie CA, Cassidy JF, Hyndman RD, Bostock MG. 2004. Shear wave anisotropy beneath the Cascadia subduction zone and western North American craton. *Geophys. J. Int.* 157:341–53

Davies JH. 1999. The role of hydraulic fractures and intermediate-depth earthquakes in generating subduction-zone magmatism. *Nature* 398:142–45

Davies JH, Stevenson DJ. 1992. Physical model of source region of subduction zone volcanics. *J. Geophys. Res.* 97:2037–70

DeShon HR, Schwartz SY. 2004. Evidence for serpentinization of the forearc mantle wedge along the Nicoya Peninsula, Costa Rica. *Geophys. Res. Lett.* 31:L21611

Eberle MA, Grasset O, Sotin C. 2002. A numerical study of the interaction between the mantle wedge, subducting slab, and overriding plate. *Phys. Earth Planet. Int.* 134:191–202

Eiler JM, ed. 2003. *Inside the Subduction Factory*. Washington, DC: Am. Geophys. Union

Elkins-Tanton LT, Grove TL, Donnelly-Nolan J. 2001. Hot, shallow mantle melting under the Cascades volcanic arc. *Geology* 29:631–34

Faul UH. 2001. Melt retention and segregation beneath mid-ocean ridges. *Nature* 410:920–23

Faul UH, FitzGerald JD, Jackson I. 2004. Shear wave attenuation and dispersion in melt-bearing olivine crystals: 2. Microstructural interpretation and seismological implications. *J. Geophys. Res.* 109:B06202

Faul UH, Jackson I. 2005. The seismological signature of temperature and grain size variations in the upper mantle. *Earth Planet. Sci. Lett.* 234:119–34

Fischer KM, Parmentier EM, Stine AR, Wolfe ER. 2000. Modeling anisotropy and plate-driven flow in the Tonga subduction zone back arc. *J. Geophys. Res.* 105:16181–91

Flanagan MP, Wiens DA. 1998. Attenuation of broadband P and S waves in Tonga: Observations of frequency dependent Q. *Pure Appl. Geophys.* 153:345–75

Fryer P, Mottl M, Johnson LE, Haggerty JA, Phipps S, Maekawa H. 1995. Serpentine bodies in the forearcs of western pacific convergent margins: Origin and associated fluids. In *Active Margins and Marginal Basins of the Western Pacific Convergent Margins*, ed. B Taylor, J Natland, pp. 259–70. Washington, DC: Am. Geophys. Union

Furukawa Y. 1993. Depth of the decoupling plate interface and thermal structure under arcs. *J. Geophys. Res.* 98:20005–13

Gaherty JB, Jordan TH, Gee LS. 1996. Seismic structure of the upper mantle in a central Pacific corridor. *J. Geophys. Res.* 10:22291–310

Gerya TV, Yuen DA, Sevre EOD. 2004. Dynamical causes for incipient magma chambers above slabs. *Geology* 32:89–92

Gorbatov A, Dominguez J, Suarez G, Kostoglodov V, Zhao D, Gordeev E. 1999. Tomographic imaging of the P-wave velocity structure beneath the Kamchatka peninsula. *Geophys. J. Int.* 137:269–79

Graeber FM, Asch G. 1999. Three-dimensional models of P wave velocity and P-to-S velocity ratio in the southern central Andes by simultaneous inversion of local earthquake data. *J. Geophys. Res.* 104:20237–56

Gribb TT, Cooper RF. 1998. Low-frequency shear attenuation in polycrystalline olivine: Grain boundary diffusion and the physical significance of the Andrade model for viscoelastic rheology. *J. Geophys. Res.* 103:27267–80

Gribb TT, Zhang S, Cooper RF. 1994. Melt migration and related attenuation in equilibrated partial melts. In *Magmatic Systems*, ed. MP Ryan, pp. 19–36. San Diego: Acad. Press

Hacker BR, Abers GA, Peacock SM. 2003. Subduction factory 1. Theoretical mineralogy, density, seismic wave speeds, and H_2O content. *J. Geophys. Res.* 108:2029

Hall CE, Gurnis M, Sdrolias M, Lavier LL, Mueller RD. 2003. Catastrophic initiation of subduction following forced convergence across fracture zones. *Earth Planet. Sci. Lett.* 212:15–30

Hall PS, Kincaid C. 2001. Diapiric flow at subduction zones; a recipe for rapid transport. *Science* 292:2472–75

Hammond WC, Humphries ED. 2000. Upper mantle seismic wave attenuation: effects of realistic partial melt distribution. *J. Geophys. Res.* 105:10987–1000

Hammond WC, Toomey DR. 2003. Seismic velocity anisotropy and heterogeneity beneath the Mantle Electromagnetic and Tomography Experiment (MELT) region of the East Pacific Rise from analysis of P and S body waves. *J. Geophys. Res.* 108:2176

Hirschmann MM, Aubaud C, Withers AC. 2005. Storage capacity of H_2O in nominally anhydrous minerals in the upper mantle. *Earth Planet Sci. Lett.* 236:167–81

Holtzman BK, Kohlstedt DL, Zimmerman ME, Heidelbach F, Hiraga T, Hustoft J. 2003. Melt segregation and strain partitioning: Implications for seismic anisotropy and mantle flow. *Science* 301:1227–30

Honda S, Saito M, Nakuki T. 2002. Possible existence of small-scale convection under the back arc. *Geophys. Res. Lett.* 29:39–42

Hsui AT, Marsh BD, Toksoez MN, Hilde TWC, Uyeda S, eds. 1983. *On Melting of the Subducted Oceanic Crust; Effects of Subduction Induced Mantle Flow*, pp. 207–20. Amsterdam: Elsevier

Hung S-H, Forsyth DW, Toomey DR. 2000. Can a narrow, melt-rich, low-velocity zone of mantle upwelling be hidden beneath the East Pacific Rise? Limits from waveform modeling and the MELT experiment. *J. Geophys. Res.* 105:7945–60

Husen S, Quintero R, Kissling E, Hacker BR. 2003. Subduction zone structure and magmatic processes beneath Costa Rica constrained by local earthquake tomography and petrological modelling. *Geophys. J. Int.* 155:11–32

Hyndman RD, Peacock SM. 2003. Serpentinization of the forearc mantle. *Earth Planet. Sci. Lett.* 212:417–32

Isaak DG. 1992. High-temperature elasticity of iron-bearing olivines. *J. Geophys. Res.* 97:1871–85

Ito Y, Obara K, Shiomi K, Sekine S, Hirosi H. Slow earthquakes coincident with episodic tremors and slow slip events. *Science* 315:503–6

Iwamori H. 1998. Tansportation of H_2O and melting in subduction zones. *Earth Planet. Sci. Lett.* 160:65–80

Jackson I. 2007. Properties of minerals and rocks—physical origins of anelasticity and attenuation in rock. In *Treatise on Geophysics*, ed. G Schubert, 2:493–526. Ansterdam: Elsevier

Jackson I, Faul UH, FitzGerald JD, Tan BH. 2004. Shear wave attenuation and dispersion in melt-bearing olivine crystals: 1. Specimen fabrication and mechanical testing. *J. Geophys. Res.* 109:B06201

Jackson I, FitzGerald JD, Faul UH, Tan BH. 2002. Grain-size-sensitive seismic wave attenuation in polycrystaline olivine. *J. Geophys. Res.* 107:B122360

Jackson I, Paterson MS, FitzGerald JD. 1992. Seismic wave dispersion and attenuation in Aheim Dunite: an experimental study. *Geophys. J. Int.* 108:517–34

Johnson MC, Plank T. 1999. Dehydration and melting experiments constrain the fate of subducted sediments. *Geochem. Geophys. Geosyst.* 1:doi:10.1029/1999GC000014

Jordan TH. 1979. Mineralogies, densities, and seismic velocities of garnet lherzolites and their geophysical significance. In *The Mantle Sample: Inclusions in Kimberlites and Other Volcanics*, ed. FR Boyd, HOA Meyer, pp. 1–14. Washington, DC: Am. Geophys. Union

Jung H, Karato S-I. 2001. Water induced fabric transitions in olivine. *Science* 293:1460–63

Jurdy DM, Stefanick M. 1983. Flow models for back-arc spreading. *Tectonophysics* 99:191–206

Kamimura A, Kasahara J, Shinohara M, Hino R, Shiobara H, et al. 2002. Crustal structure study at the Izu-Bonin subduction zone around 31N: implications of serpentinized materials along the subduction boundary. *Phys. Earth Planet. Int.* 132:105–29

Kaminski E, Ribe NM, Browaeys JT. 2004. D-Rex, a program for calculation of seismic anisotropy due to crystal lattice preferred orientation in the convective upper mantle. *Geophys. J. Int.* 158:744–52

Karato S-I. 1993. Importance of anelasticity in the interpretation of seismic tomography. *Geophys. Res. Lett.* 20:1623–26

Karato S-I. 2003. Mapping water content in the upper mantle. See Eiler 2003, pp. 135–52

Katayama I, Karato S-I. 2006. Effect of temperature on the B- to C-type olivine fabric transition and implication for flow pattern in subduction zones. *Phys. Earth Planet. Int.* 157:33–45

Katz RF. 2002. *Models of equilibrium and reactive melting in a subduction zone setting*. Master's thesis. Columbia Univ., New York

Kelemen PB, Rilling JL, Parmentier EM, Mehl L, Hacker BR. 2003. Thermal structure due to solid-state flow in the mantle wedge beneath arcs. See Eiler 2003, pp. 293–311

Kelley KA, Plank T, Grove TL, Stolper EM, Newman S, Hauri E. 2006. Mantle melting as a function of water content beneath back-arc basins. *J. Geophys. Res.* 111:B09208

Kennett BLN, Engdahl ER. 1991. Traveltimes for global earthquake location and phase identification. *Geophys. J. Int.* 105:429–65

Kincaid C, Griffiths RW. 2003. Laboratory models of the thermal evolution of the mantle during rollback subduction. *Nature* 425:58–62

Kincaid C, Sacks IS. 1997. Thermal and dynamical evolution of the upper mantle in subduction zones. *J. Geophys. Res.* 102:12295–316

Kneller EA, van Keken PE. 2006. The effects of 3D slab geometry on deformation in the mantle wedge. *EOS Trans. Am. Geophys. Union* 87(52):T22C-07

Kneller EA, van Keken PE, Karato S-I, Park J. 2005. B-type olivine fabric in the mantle wedge: insights from high-resolution non-Newtonian subduction zone models. *Earth Planet. Sci. Lett.* 237:781–97

Lassak TM, Fouch MJ, Hall CE, Kaminski E. 2006. Seismic characterization of mantle flow in subduction systems: Can we resolve a hydrated mantle wedge? *Earth Planet. Sci. Lett.* 243:632–49

Lee C-TA. 2003. Compositional variation of density and seismic velocities in natural peridotites at STP conditions: implications for seismic imaging of compositional heterogeneities in the upper mantle. *J. Geophys. Res.* 108:B92441

Levin V, Droznin D, Park J, Gordeev E. 2004. Detailed mapping of seismic anisotropy with local shear waves in southeastern Kamchatka. *Geophys. J. Int.* 158:1009–23

Liang Y, Price JD, Wark DA, Watson EB. 2001. Nonlinear pressure diffusion in a porous medium: approximate solutions with applications to permeability measurements using transient pulse decay method. *J. Geophys. Res.* 106:529–35

Long MD, Van Der Hilst R. 2005. Upper mantle anisotropy beneath Japan from shear wave splitting. *Phys. Earth Planet. Int.* 151:206–22

Long MD, Van Der Hilst R. 2006. Shear wave splitting from local events beneath the Ryukyu arc: Trench parallel anisotropy in the mantle wedge. *Phys. Earth Planet. Int.* 155:300–12

Lundstrom CC, Gill J, Williams Q. 1998. Investigating solid mantle upwelling beneath mid-ocean ridges using U-series disequilibria. I. A global approach. *Earth Planet. Sci. Lett.* 157:151–65

Mainprice D, Silver PG. 1993. Interpretation of SKS-waves using samples from the subcontinental mantle. *Phys. Earth Planet. Int.* 78:257–80

Mavko GM. 1980. Velocity and attenuation in partially molten rocks. *J. Geophys. Res.* 85:5173–89

Mavko GM, Nur A. 1975. Velocity and attenuation in partially molten rocks. *J. Geophys. Res.* 80:1444–48

Mei S, Kohlstedt DL. 2000a. Influence of water of plastic deformation of olivine aggregates: 1. Diffusion creep regime. *J. Geophys. Res.* 105:21457–69

Mei S, Kohlstedt DL. 2000b. Influence of water of plastic deformation of olivine aggregates: 2. Dislocation creep regime. *J. Geophys. Res.* 105:21471–81

Mibe K, Fujii T, Yasuda A. 1999. Control of the location of the volcanic front in island arcs by aqueous fluid connectivity in the mantle wedge. *Nature* 401:259–62

Myers SC, Beck S, Zandt G, Wallace T. 1998. Lithospheric-scale structure across the Bolivian Andes from tomographic images of velocity and attenuation for P and S waves. *J. Geophys. Res.* 103:21233–52

Nakajima J, Hasagawa A. 2004. Shear-wave polarization anisotropy and subduction-induced flow in the mantle wedge of northeastern Japan. *Earth Plan. Sci. Lett.* 225:365–77

Nakajima J, Matsuzawa T, Hasegawa A, Zhao D. 2001. Three-dimensional structure of V_p, V_s, and V_p/V_s beneath northeastern Japan: Implications for arc magmatism and fluids. *J. Geophys. Res.* 106:21843–57

Nakajima J, Shimizu J, Hori S, Hasagawa A. 2006. Shear-wave splitting beneath the southwestern Kurile arc and northeastern Japan arc: A new insight into mantle return flow. *Geophys. Res. Lett.* 33:L05305

Nakajima J, Takei Y, Hasegawa A. 2005. Quantitative analysis of the inclined low-velocity zone in the mantle wedge of Northeastern Japan: a systematic change of melt-filled pore shapes with depth and its implications for melt migration. *Earth Planet. Sci. Lett.* 234:59–70

Nishimura C, Forsyth DW. 1989. The anisotropic structure of the upper mantle in the Pacific Ocean. *Geophys. J.* 96:203–29

O'Connell RJ, Budiansky B. 1974. Seismic velocities in dry and saturated cracked solids. *J. Geophys. Res.* 79:5412–26

O'Connell RJ, Budiansky B. 1977. Viscoelastic properties of fluid-saturated cracked solids. *J. Geophys. Res.* 82:5719–35

Ono S. 1998. Stability limits of hydrous minerals in sediment and mid-ocean ridge basalt compositions; implications for water transport in subduction zones. *J. Geophys. Res.* 103:18253–67

Peacock SM, Rushmer T, Thompson AB. 1994. Partial melting of subducting oceanic crust. *Earth Planet. Sci. Lett.* 121:227–44

Pearce JA, Stern RJ. 2006. The origin of Back-arc basin magmas: Trace element and isotope perspectives. In *Back-arc Spreading Systems—Geological, Biological, Chemical, and Physical Interactions*, ed. DM Christie, CR Fisher, S-M Lee, S Givens, pp. 63–86. Washington, DC: Am. Geophys. Union

Poirier J-P. 1985. *Creep of Crystals. High-Temperature Deformation Processes in Metals Ceramics and Minerals*. Cambridge, UK: Cambridge Univ. Press
Pozgay SH, Wiens DA, Conder JA, Shiobara H, Sugioka H. 2007a. Complex mantle flow in the Mariana subduction system: Evidence from shear wave splitting. *Geophys. J. Int.* 170:371–86
Pozgay SH, Wiens DA, Conder JA, Shiobara H, Sugioka H, 2007b. Seismic attenuation structure of the Mariana subduction system. *EOS Trans. Am. Geophys. Union* 88:T43C-04
Raj R, Ashby MF. 1971. On grain boundary sliding and diffusional creep. *Metal. Trans.* 2:1113–27
Renner J, Viscupic K, Hirth G, Evans B. 2003. Melt extraction from partially molten peridotites. *Geochem. Geophys. Geosyst.* 4:doi:10.1029/2002GC000369
Reyners M. 2006. Imaging subduction from the trench to 300 km depth beneath the central North Island, New Zealand with V_p and V_p/V_s. *Geophys. J. Int.* 165:565–83
Ribe NM. 1989. Mantle flow induced by back arc spreading. *Geophys. J. Int.* 98:85–91
Rivers ML, Carmichael ISE. 1987. Ultrasonic studies of silicate melts. *J. Geophys. Res.* 92:9247–70
Rogers G, Dragert H. 2003. Episodic tremor and slip on the Cascadia Subduction Zone: the chatter of silent slip. *Science* 300:1942–43
Romanowicz B. 1995. A global tomographic model of shear attenuation in the upper mantle. *J. Geophys. Res.* 100:12375–94
Roth EG, Wiens DA, Dorman LM, Hildebrand J, Webb SC. 1999. Seismic attenuation tomography of the Tonga-Fiji region using phase pair methods. *J. Geophys. Res.* 104:4795–810
Schmeling H. 1985. Numerical models on the influence of partial melt on elastic, anelastic and electric properties of rocks. Part I: elasticity and anelasticity. *Phys. Earth Planet. Int.* 41:34–57
Schmidt MW, Poli S. 1998. Experimentally based water budgets for dehydrating slabs and consequences for arc magma generation. *Earth Planet. Sci. Lett.* 163:361–79
Schurr B, Asch G, Rietbrock A, Trumbull RB, Haberland C. 2003. Complex patterns of fluid and melt transport in the central Andean subduction zone revealed by attenuation tomography. *Earth Planet. Sci. Lett.* 215:105–19
Schutt DL, Lesher CE. 2006. The effects of melt depletion on the density and seismic velocity of garnet and spinel lherzolite. *J. Geophys. Res.* 111:B05401
Scott DR, Stevenson DJ. 1989. A self-consistent model of melting, magma migration, and buoyancy-driven circulation beneath mid-ocean ridges. *J. Geophys. Res.* 94:2973–88
Shen Y, Forsyth DW. 1995. Geochemical constraints on initial and final depths of melting beneath mid-ocean ridges. *J. Geophys. Res.* 100:2211–38
Shito A, Karato S-I, Matsukage KN, Nishihara Y. 2006. Towards mapping the three-dimensional distribution of water in the upper mantle from velocity and attenuation tomography. In *Earth's Deep Water Cycle*, ed. SD Jacobsen, S van der Lee. Washington, DC: Am. Geophys. Union
Shito A, Karato S-I, Park J. 2004. Frequency dependence of Q in Earth's upper mantle inferred from continuous spectra of body waves. *Geophys. Res. Lett.* 31:L12603

Sisson TW, Bronto S. 1998. Evidence for pressure-release melting beneath magmatic arcs from basalt at Galunggung, Indonesia. *Nature* 391:883–86
Sleep NH, Toksoz MN. 1971. Evolution of marginal basins. *Nature* 33:548–50
Smith GP, Wiens DA, Fischer KM, Dorman LM, Webb SC, Hildebrand JA. 2001. A complex pattern of mantle flow in the Lau backarc. *Science* 292:713–16
Stachnik JC, Abers GA, Chistensen DH. 2004. Seismic attenuation and mantle wedge temperatures in the Alaska subduction zone. *J. Geophys. Res.* 109:B10304
Takanami T, Sacks IS, Hasegawa A. 2000. Attenuation structure beneath the volcanic front in northeastern Japan from broad-band seismograms. *Phys. Earth Planet. Int.* 121:339–57
Takei Y. 1998. Constitutive mechanical relations of solid-liquid composites in terms of grain-boundary contiguity. *J. Geophys. Res.* 103:18183–203
Takei Y. 2000. Acoustic properties of partially molten media studied on a simple binary system with controllable dihedral angle. *J. Geophys. Res.* 105:16665–82
Takei Y. 2002. Effect of pore geometry on V_P/V_S: from equilibrium geometry to crack. *J. Geophys. Res.* 107:doi:10.1029/2001JB000522
Tamura Y, Tatsumi Y, Zhao D, Kido Y, Shukuno H. 2002. Hot fingers in the mantle wedge: new insights into magma genesis in subduction zones. *Earth Plan. Sci. Lett.* 197:105–16
Tan BH, Jackson I, FitzGerald JD. 1997. Shear wave dispersion and attenuation in fine-grained synthetic olivine aggregates: Preliminary results. *Geophys. Res. Lett.* 24:1055–58
Tatsumi Y. 1989. Migration of fluid phases and genesis of basalt magmas in subduction zones. *J. Geophys. Res.* 94:4697–707
Tatsumi Y. 2005. The subduction factory: how it operates in the evolving earth. *GSA Today* 15:4–10
Taylor B, Karner GD. 1983. On the evolution of marginal basins. *Rev. Geophys. Space Phys.* 21:1727–41
Taylor B, Martinez F. 2003. Back-arc basin basalt systematics. *Earth Planet. Sci. Lett.* 210:481–97
Thompson AB. 1992. Water in the earth's upper mantle. *Nature* 358:295–302
Tichelaar BW, Ruff LJ. 1993. Depth of seismic coupling along subduction zones. *J. Geophys. Res.* 98:2017–37
Tsumura N, Matsumoto S, Horiuchi S, Hasegawa A. 2000. Three-dimensional attenuation structure beneath the northeastern Japan arc estimated from spectra of small earthquakes. *Tectonophysics* 319:241–60
Turcotte DL, Morgan JP. 1993. The physics of magma migration and mantle flow beneath a mid-ocean ridge. In *Mantle Flow and Melt Generation at Mid-Ocean Ridges*, ed. Morgan JP, Blackman DK, Sinton JM, pp. 155–82. Washington, DC: Am. Geophys. Union
Turner S, Hawkesworth C. 1998. Using geochemistry to map mantle flow beneath the Lau basin. *Geology* 26:1019–22
Turner S, Regelous M, Hawkesworth C, Rostami K. 2006. Partial melting processes above subducting plates: constraints from 231Pa–235U disequilibria. *Geochim. Cosmochim. Acta* 70:480–503

Turner SP, George RMM, Evans PJ, Hawkesworth CJ, Zellmer GF. 2000. Timescales of magma formation, ascent and storage beneath subduction-zone volcanoes. *Philos. Trans. R. Soc. London Ser. A* 358:1443–64

van Keken PE. 2003. The structure and dynamics of the mantle wedge. *Earth Planet. Sci. Lett.* 215:323–38

Waff HS, Bulau JR. 1979. Equilibrium fluid distribution in an ultramafic partial melt under hydrostatic conditions. *J. Geophys. Res.* 84:6109–14

Wagner LS, Beck S, Zandt G. 2005. Upper mantle structure in the south central Chilean subduction zone (30–36 S). *J. Geophys. Res.* 110:B01308

Wark DA, Watson EB. 1998. Grain scale permeabilities of texturally equilibrated, monomineralic rocks. *Earth Planet. Sci. Lett.* 164:591–605

Wiens DA, Kelley K, Plank T. 2006a. Mantle temperature variations beneath backarc spreading centers inferred from seismology, petrology, and bathymetry. *Earth Planet. Sci. Lett.* 248:30–42

Wiens DA, Seama N, Conder JA. 2006b. Mantle structure and flow patterns beneath active backarc basins inferred from passive seismic and electromagnetic methods. In *Interactions among Physical, Chemical, Biological, and Geological Processes in Back-Arc Spreading Systems*, ed. DM Christie, CR Fisher, S-M Lee, S Givens, pp. 43–62. Washington, DC: Am. Geophys. Union

Wiens DA, Smith GP. 2003. Seismological constraints on structure and flow patterns within the mantle wedge. See Eiler 2003, pp. 58–81

Yang X, Fischer KM, Abers GA. 1995. Seismic anisotropy beneath the Shumagin Islands segment of the Aleutian-Alaska subduction zone. *J. Geophys. Res.* 100:18165–78

Zhang S, Karato S. 1995. Lattice preferred orientation of olivine agregates deformed in simple shear. *Nature* 375:774–77

Zhao D, Christensen D, Pulpan H. 1995. Tomographic imaging of the Alaska subduction zone. *J. Geophys. Res.* 100:6487–504

Zhao D, Hasegawa A. 1993. P wave tomographic imaging of the crust and upper mantle beneath the Japan Islands. *J. Geophys. Res.* 98:4333–53

Zhao D, Hasegawa A, Horiuchi S. 1992. Tomographic imaging of P and S wave velocity structure beneath Northeastern Japan. *J. Geophys. Res.* 97:19909–28

Zhao D, Wang Z, Umino N, Hasagawa A. 2007. Tomographic imaging outside a seismic network: Application to the Northeast Japan arc. *Bull. Seismol. Soc. Am.* 97:1121–32

Zhao D, Xu Y, Wiens DA, Dorman L, Hildebrand J, Webb S. 1997. Depth extent of the Lau back-arc spreading center and its relationship to the subduction process. *Science* 278:254–57

Zhong S, Gurnis M. 1995. Mantle convection with plates and mobile, faulted plate margins. *Science* 267:838–43

Annual Review
of Earth and
Planetary Sciences
Volume 36, 2008

Contents

Indexes

Errata

An online log of corrections to *Annual Review of Earth and Planetary Sciences* articles may be found at http://earth.annualreviews.org